POLITECNICO
MILANO 1863

SCUOLA DI INGEGNERIA INDUSTRIALE
E DELL'INFORMAZIONE

Long-term Energy Planning Analyses for *Empresa Siderúrgica del Mutún*: Natural Gas, Renewables and Small Modular Reactor

Tesi di Laurea Magistrale in
Energy Engineering - Energy for Development

Author: **Claudia Tancredi**

Student ID: 252801
Advisor: Prof. Nicolò Stevanato
Co-advisors: Tommaso Zacconi
Academic Year: 2025-26

Abstract

This thesis investigates the decarbonization pathways for *Empresa Siderúrgica del Mutún*, a greenfield steel plant located in the Mutún region (Bolivia), by developing an energy-system modeling framework that consistently represents steelmaking pathways. The reference (baseline) case assumes a conventional energy supply in which natural gas provides the full energy input to the plant. Alternative scenarios are assessed against this baseline through two main levers.

First, the study evaluates the integration of hydrogen in the Direct Reduced Iron (DRI) route, which intrinsically reduces process-related CO_2 emissions by partially or fully substituting fossil-based reducing agents. Second, the work explores different portfolios of electricity supply to produce low-carbon hydrogen and meet the electrical demand of the plant. These portfolios combine renewable energy sources and/or a Small Modular Reactor (SMR) as firm low-carbon generation. In line with the scope of the work, the analysis focuses on the electrical domain, while thermal demands are assumed to remain outside the decarbonization options considered.

The modeling approach enables a consistent comparison of technological configurations and operational strategies, quantifying their implications in terms of energy balances and emissions performance relative to the baseline based on natural-gas. The results support strategic decision-making for the Mutún project by clarifying the role of hydrogen-based DRI and the potential contribution of renewables and SMRs to deep decarbonization of the steel supply chain.

Abstract in lingua italiana

Questa tesi ha l'obiettivo di analizzare diversi percorsi di decarbonizzazione per la *Empresa Siderúrgica del Mutún*, un impianto siderurgico situato nella regione del Mutún, in Bolivia. L'analisi si basa su un approccio di energy system modelling finalizzato alla valutazione di scenari alternativi, con lo scopo di individuare le configurazioni in grado di garantire le minori emissioni di CO_2 compatibilmente con le caratteristiche dell'impianto.

Il caso di riferimento (baseline) assume l'utilizzo del gas naturale come unica fonte di approvvigionamento energetico per soddisfare l'intera domanda dell'impianto. A partire da questo scenario, vengono analizzate configurazioni alternative articolate su due principali livelli di intervento.

In primo luogo, lo studio valuta l'integrazione dell'idrogeno nel processo di Direct Reduced Iron (DRI), che consente una riduzione delle emissioni di CO_2 attraverso la sostituzione parziale o totale degli agenti riducenti di origine fossile. In secondo luogo, vengono esaminate soluzioni a minore impatto ambientale per la copertura della domanda energetica elettrica dell'impianto, che possono al contempo costituire una risorsa per la produzione di idrogeno. In questo contesto, vengono considerate sia l'integrazione di fonti energetiche rinnovabili (Renewable Energy Sources, RES) sia la possibilità di installare uno Small Modular Reactor (SMR) in prossimità del sito industriale.

L'approccio modellistico adottato consente di confrontare in modo coerente le diverse tecnologie e strategie operative, valutandone le prestazioni in termini di bilancio energetico ed emissioni rispetto al caso di riferimento basato sul gas naturale. I risultati ottenuti forniscono un supporto al processo decisionale per *Empresa Siderúrgica del Mutún*, chiarendo il ruolo dell'idrogeno nel processo DRI e il potenziale contributo delle fonti rinnovabili e dell'energia nucleare nella decarbonizzazione della filiera produttiva dell'acciaio.

Contents

Abstract **i**

Abstract in lingua italiana **iii**

Contents **v**

1 Introduction **1**

2 Industrial Decarbonization Challenge in Hard-to-Abate Sectors **5**
2.1 Steel Industry and Energy-Intensive Processes 5
2.2 A Possible Pathway in Steelmaking Decarbonization: H_2-DRI 8
2.2.1 Hydrogen integration in the DRI route 9
2.2.2 Possible H_2-DRI configuration Scenarios 10
2.3 Object of the thesis 13

3 Materials and Methods **15**
3.1 Hypatia framework and model structure 15
3.2 Timeseries clustering 19
3.3 Modelling of Nuclear Reactor cogeneration 23

4 Case Study: Empresa Siderúrgica del Mutún **27**
4.1 Territorial resources: solar, wind and water 27
4.1.1 Solar resource 28
4.1.2 Wind resource 28
4.1.3 Water resources 29
4.2 Plant Characterization 29
4.2.1 Plant energy demand: electricity and heat 30
4.2.2 Water Consumptions and Utilities 33
4.3 Scenario Selection 34
4.4 Reference Energy System 35

4.5 H_2 Demand for DRI Conversion 37

5 Results **39**

5.1 Environmental impact analysis 42
5.2 Economic comparison 44
5.3 Carbon credits as a potential pathway 46
5.4 Energy security and supply diversification 49
5.5 Land availability and spatial constraints 51
5.6 Sensitivity Analysis of SMR Investment Costs 52
5.7 Discussion 54

6 Conclusions **57**

Bibliography **61**

A Appendix A **67**

B Appendix B **69**

List of Figures **71**

List of Tables **73**

Acknowledgements **75**

1 | Introduction

Steel plays an essential role in modern society as a key material for construction, transportation, machinery, and energy infrastructure. Its versatility, strength, and recyclability make it one of the most important industrial materials in use today. As a result, global steel demand is expected to remain significant in the coming decades, driven by population growth, urbanisation, and economic development.

Steel is also a critical enabler of the energy transition. It is required for wind turbines, solar panels and dam construction for hydropower, to electric vehicle components including electrical steel for motors, as well as storage (both for renewable energy and carbon capture) [7].

However, steelmaking remains energy- and carbon-intensive. According to the International Energy Agency (IEA), the sector accounts for around 8% of global final energy demand and approximately 7% of total energy-related CO_2 emissions [24]. These emissions are largely associated with fossil fuel use and the reliance on carbon-based reducing agents in conventional steelmaking routes, particularly the blast furnace-basic oxygen furnace (BF-BOF) process, which remains predominant with 70% of global crude steel produced using this process.

This highlights the need to decarbonize the sector through innovations in both production processes and energy supply systems.

Recent studies have investigated several pathways to low-carbon steel, including increased scrap utilisation with electric arc furnaces (EAF), hydrogen-based direct reduction (H_2-DRI), carbon capture and storage (CCS), and the integration of low-carbon electricity from renewable or nuclear sources [24].

In particular, using hydrogen, produced via electrolysis powered by renewable sources or nuclear power, to make DRI followed by steel production using an EAF can reduce emissions to almost zero compared to the BF-BOF. Figure 1.1 compares the conventional BF-BOF route with the Direct Reduction - EAF and H_2-Direct Reduction - EAF routes. It highlights the shift from fossil-based reductants to hydrogen, and the role of low-carbon

electricity to produce H_2 via electrolysis.

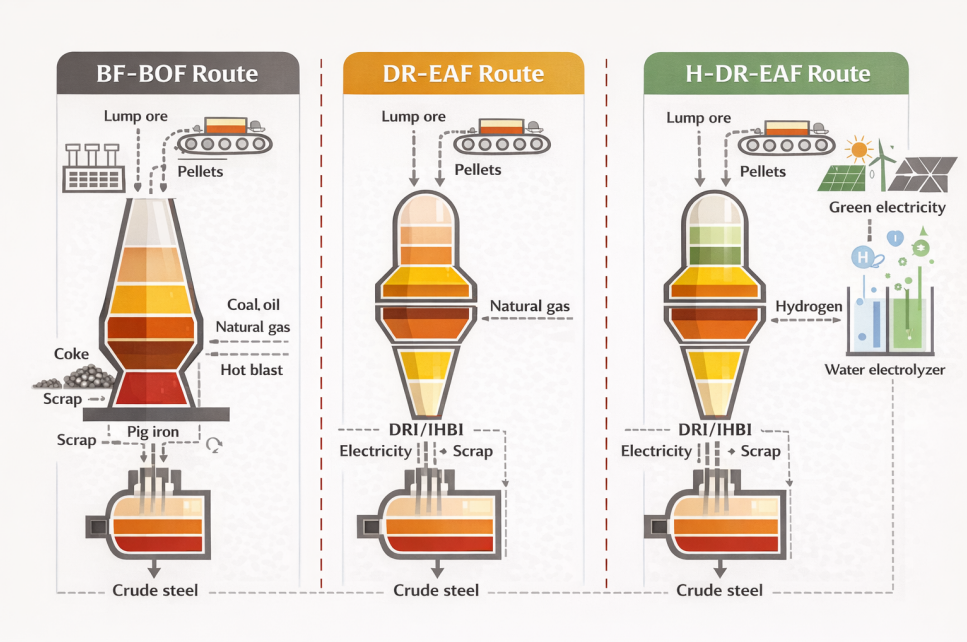

Figure 1.1: Schematic comparison of the BF–BOF, DR–EAF, and H–DR–EAF steelmaking routes [11].

The purpose of this study is to analyse the energy demand and supply structure of the *Empresa Siderúrgica del Mutún* (ESM), a steel plant located in Bolivia, Latin America. The analysis examines the potential introduction of a H_2–DRI–EAF configuration and investigates how the current natural-gas-based energy mix could be diversified or partially replaced with low-carbon energy sources, including renewable and nuclear options. In doing so, the study explicitly considers the cost–emissions trade-off associated with deep decarbonisation across the plant's alternative development pathways. The assessment is carried out over multiple development steps to reflect the planned evolution of production and technology deployment, and to quantify the implications of alternative energy supply configurations in terms of energy balances and CO_2 emissions.

The study begins with an overview of the main steel production stages and their corresponding energy requirements, followed by a review of the available decarbonisation pathways, with a particular focus on hydrogen-based routes. An energy system modeling framework is then presented, explaining how it is used to explore alternative energy supply configurations and evaluate their performance under different scenarios. Plant-specific information for the *Empresa Siderúrgica del Mutún* is used to define modeling assumptions and to estimate energy intensities, production growth, and scenario parameters.

Overall, this work contributes to the broader debate on decarbonising hard-to-abate sectors by illustrating how energy supply choices can support cleaner and more resilient steelmaking pathways in developing economies.

2 | Industrial Decarbonization Challenge in Hard-to-Abate Sectors

This section addresses the challenge of industrial decarbonization in sectors that are hard-to eliminate, focusing on the steel industry. First, the main stages of the steelmaking process are described together with their energy use. The section then introduces the main decarbonization pathways discussed in the literature, with particular attention to process and energy supply solutions that could be integrated in the case study. Finally, the current configuration of the selected case study is presented, and the objectives of this research are defined.

2.1. Steel Industry and Energy-Intensive Processes

The steelmaking process is characterized by some fundamental production steps, each associated with an energy demands and consumption patterns. A clear overview of these stages is crucial to identify which parts of the production chain are responsible for the highest energy use and represent the most critical targets for decarbonization strategies.

Ore Concentration

Steel production consists of a sequence of interconnected stages that follow one another along the production chain. The first of these stages is the concentration process. During this phase, raw iron ore is crushed, ground, and subsequently enriched in order to increase its iron content and remove unwanted impurities. This stage is predominantly mechanical in nature and typically involves the use of crushing and grinding mills, as well as magnetic or chemical separation technologies. Although the concentration process does not require significant thermal energy input, it entails a substantial consumption of electrical energy, mainly associated with material handling [37].

Pelletizing

The concentrated iron ore is subsequently processed into durable spherical pellets. In this stage, the concentrate is blended with selected additives, such as anthracite, dolomite, and binding agents, to achieve the required chemical composition and particle size distribution. The prepared mixture is then shaped into so-called green pellets, typically with diameters ranging from 8 to 16 mm, through a purely mechanical process that does not involve thermal energy consumption [17].

These green pellets are subsequently subjected to an induration process in high-temperature furnaces, where thermal treatment provides the mechanical strength and metallurgical characteristics necessary for handling and downstream reduction. Based on the available data, temperatures of up to 1350 °C are required during this final hardening phase [17]. While the electrical energy demand of this stage is relatively limited, it constitutes one of the most energy-intensive steps in terms of thermal energy consumption.

Direct Reduced Iron (DRI)

Once the pelletizing stage is completed, the iron ore pellets enter the shaft furnace , where iron oxides (Fe_2O_3) are reduced to solid metallic iron (Fe) at high temperatures, without reaching the melting point.[1] The reduction is achieved by a hot reducing gas, mainly composed of hydrogen (H_2) and carbon monoxide (CO), according to the following reactions[35]:

$$Fe_2O_3 + 3CO \rightarrow 2Fe + 3CO_2, \qquad \Delta H^{\circ}_{25^{\circ}C} = -25 \text{ kJ} \tag{2.1}$$

$$Fe_2O_3 + 3H_2 \rightarrow 2Fe + 3H_2O, \qquad \Delta H^{\circ}_{25^{\circ}C} = +99 \text{ kJ} \tag{2.2}$$

Natural gas plays a dual role during this stage of the process. Firstly, it is used as feedstock for the production of the reducing gas through the steam reforming reaction:

$$CH_4 + H_2O \rightarrow CO + 3H_2 \tag{2.3}$$

Secondly, natural gas is combusted to supply the thermal energy required by both the shaft furnace and the reformer. Maintaining the operating temperature at approximately 1100 °C requires a substantial heat input [35]. As a result, natural gas acts simultaneously as an *energy carrier* and as a *chemical reducing agent* within the direct reduction process.

[1] The melting point of pure iron is 1538 °C.

Electric Arc Furnace (EAF)

Following the direct reduction stage, the steelmaking phase takes place. This step can be carried out through different technological routes. The most common configuration worldwide is based on the blast furnace, which is still employed in the majority of conventional integrated steel plants. However, in recent years, more innovative solutions have gained increasing attention, particularly in the context of CO_2 emission reduction strategies. In the process configuration considered in this study, steel production is performed using an Electric Arc Furnace (EAF).

In this configuration, the direct reduced iron (DRI), also referred to as sponge iron, is melted in the EAF. Scrap metal may be added to the charge, and refining operations are carried out in order to obtain liquid steel with the desired chemical composition. The process is primarily driven by electrical energy, supplied through high-voltage electric arcs, although a thermal contribution is also required for auxiliary systems such as material preheating, off-gas post-combustion, and refractory wall heating.

The EAF operates by generating an electric arc between three consumable graphite electrodes and the metallic charge, with the electrodes entering the furnace from the top. During this stage, the highest temperatures of the entire steelmaking process are reached, up to approximately 1650 °C, making the steel mill phase the hottest section of the production chain [32].

Rolling Mill

Following the steelmaking stage, the process continues with the rolling mill phase. After solidification, steel semi-finished products are reheated in dedicated furnaces to the rolling temperature, typically in the range of 1000 °C to 1300 °C. Once the target temperature is reached, the material is passed through a series of rolling stands, where its cross-sectional area is progressively reduced to obtain the desired final geometry.

The rolling mill is characterized by a significant thermal energy demand associated with the reheating furnaces, while the deformation process itself is predominantly mechanical, driven by electric motors and rolling stands [39]

Figure 2.1 shows the main steps of the steel production route considered in this study, which are described in greater detail later in the text.

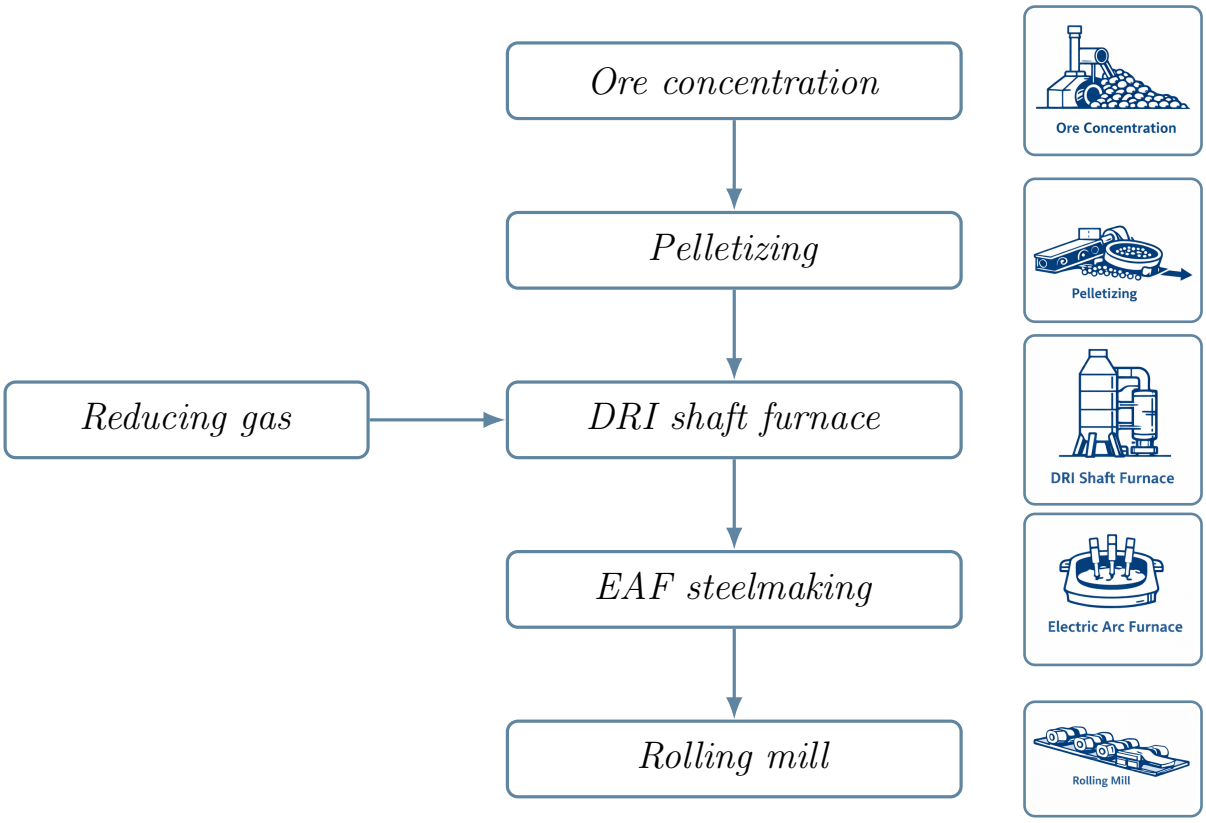

Figure 2.1: Simplified steelmaking route with representative equipment sketches for each process step.

2.2. A Possible Pathway in Steelmaking Decarbonization: H_2-DRI

After presenting the main stages of the steelmaking process and identifying the need to reduce the associated CO_2 emissions, several decarbonization pathways can be considered. These include the increased use of scrap and electric arc furnaces, the application of carbon capture and storage (CCS) technologies, process electrification, and the adoption of alternative reducing agents [30]. Among these options, hydrogen-based solutions have gained increasing attention in recent years due to their potential to significantly reduce process-related emissions in iron and steel production [41].

Hydrogen already plays an important role in conventional natural-gas-based direct reduction (NG-DRI) systems: it is generated through steam reforming of natural gas and constitutes a considerable fraction of the reducing gas mixture [35]. However, in this configuration, the hydrogen is still indirectly associated with fossil fuel use and CO_2 emissions.

An alternative pathway, which is the focus of this work, is hydrogen-based direct reduced iron (H_2-DRI). In this case, hydrogen is externally produced and supplied directly to the shaft furnace as the primary reducing agent. By replacing carbon-based reductants, this route enables a substantial reduction in process-related CO_2 emissions [11].

The actual decarbonization potential of H_2-DRI strongly depends on the method used for hydrogen production. To achieve meaningful emission reductions, hydrogen must be produced using low-carbon electricity sources, such as renewable or nuclear energy. In this sense, hydrogen-based steelmaking leads to a dual mitigation effect: on the one hand, it reduces emissions within the reduction process itself; on the other hand, it creates an opportunity to integrate low-carbon power sources that can also contribute to the overall electrical demand of the steel plant.

For these reasons, this study builds on these efforts by analyzing the role of hydrogen integration with particular attention to its interaction with different low-carbon electricity supply options.

2.2.1. Hydrogen integration in the DRI route

The direct reduced iron (DRI) process considered in this study is based on ENERGIRON shaft furnace technology. In this configuration, iron ore is reduced using a hot reducing gas composed primarily of hydrogen and carbon monoxide.

In conventional natural-gas-based operation, the reducing gas is generated through steam reforming of natural gas in a dedicated reformer unit. The resulting gas mixture typically contains approximately 55% H_2 and 36% CO, together with smaller fractions of CH_4, CO_2, H_2O, and N_2. Owing to this composition, the process already operates under hydrogen-rich conditions, which facilitates the integration of additional hydrogen into the reduction stage [19].

When transitioning toward hydrogen-based operation, the dominant reduction reaction progressively shifts toward:

$$Fe_2O_3 + 3H_2 \rightarrow 2Fe + 3H_2O$$

In contrast to carbon-based reduction reactions, this pathway does not generate direct CO_2 emissions at the reduction stage, as water vapor is the only reaction by-product. The schematics of the two configurations are shown in Fig. 2.2.

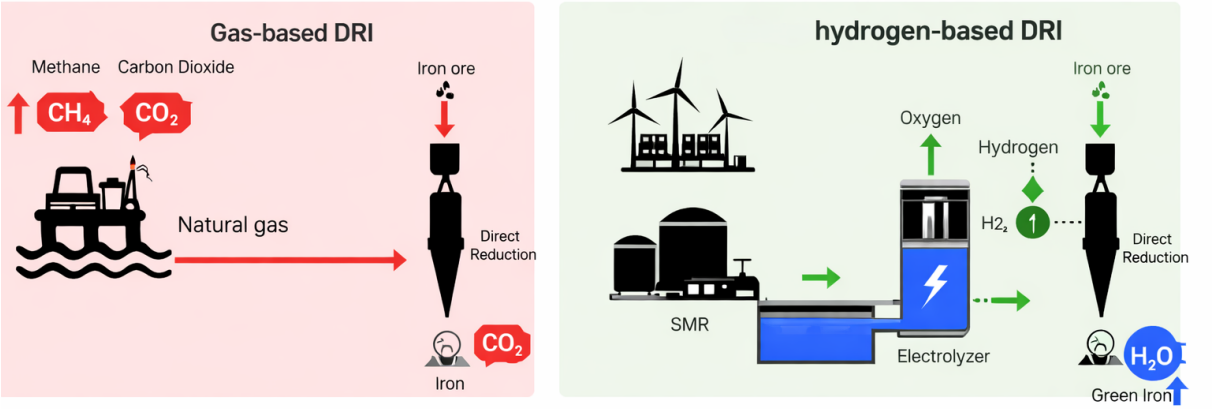

Figure 2.2: Natural gas-based DRI and Pink/Green Hydrogen-based DRI configurations [3].

Hydrogen can be progressively introduced as a reducing agent, allowing partial substitution of natural gas in existing DRI plants before reaching full hydrogen-based operation. According to ENERGIRON [19], up to 30% of the natural gas input can currently be substituted with externally supplied hydrogen without requiring major modifications to the shaft furnace or the core process layout. In this partial substitution configuration, hydrogen is blended into the existing reducing gas circuit, coexisting with reformer-derived gas. Due to the already hydrogen-rich atmosphere of the furnace, this approach does not significantly affect the reduction kinetics or the overall thermal balance of the process.

However, achieving full hydrogen-based operation (100% H_2) requires additional technical adaptations. Since hydrogen-based reduction is highly endothermic, the injected hydrogen must be preheated to temperatures of approximately 900 °C before entering the shaft furnace. Because of that, the installation of a dedicated hydrogen preheating system is necessary, as well as upgrades to auxiliary components such as valves, seals, and piping [19].

Therefore, in this study, the fully hydrogen-based configuration (100% H_2) is not investigated.

2.2.2. Possible H_2-DRI configuration Scenarios

After establishing the technical feasibility of hydrogen integration within the DRI process, the next step is to investigate how this transition can be implemented in practice. This requires analyzing the different system configurations through which hydrogen can be supplied to the DRI–EAF route.

As briefly introduced in the previous sections, the potential decarbonization of hydrogen-based steelmaking does not solely depend on its use as a reducing agent, but is strongly influenced by the way hydrogen is produced. For this reason, the analysis must extend beyond the DRI process and include the upstream energy sources used for hydrogen generation, which ultimately determine the overall emission performance of the system.

In this context, two main hydrogen production pathways are considered, representing different H_2-DRI-EAF configuration scenarios. These pathways are selected based on their relevance in current research and industrial practice, as well as their potential compatibility with low-carbon energy systems.

Renewable Energy Source

The first hydrogen production configuration relies on renewable energy sources, which are used both to meet the electricity demand and to produce hydrogen via water electrolysis. In particular, low-temperature water electrolysis using Proton Exchange Membrane (PEM) electrolyzers is considered.

PEM electrolysis operates at temperatures of approximately 70 °C and features a fast dynamic response, allowing an effective integration with fluctuating power input conditions [29].

The electrochemical reactions that occur in a PEM electrolyzer are reported below:

$$\text{Anode (oxidation):} \quad 2H_2O \rightarrow O_2 + 4H^+ + 4e^-$$

$$\text{Cathode (reduction):} \quad 4H^+ + 4e^- \rightarrow 2H_2$$

$$\text{Overall reaction:} \quad 2H_2O \rightarrow 2H_2 + O_2$$

As already underlined, the total installed renewable capacity will be primarily used for hydrogen production and will also contribute to meeting the electricity demand of the plant.

Small Modular Reactor

The other potential decarbonisation option is the deployment of a Small Modular Reactor (SMR).

SMRs are advanced nuclear systems characterised by a lower electrical output (typically below 300 MWe) and modular construction. Despite their smaller size, they operate according to the same fundamental principles as conventional nuclear power plants: nuclear

fission releases heat, which is transferred to a working fluid and converted into electricity through a steam cycle and a turbine-generator set [31].

Due to their compact design, SMRs often rely on enhanced and partially passive safety features and can be manufactured in a factory setting, reducing the construction time and associated costs on-site. As a result, they are generally associated with simplified plant layouts, improved safety, and lower initial investment requirements compared to large reactors [31].

A key aspect for this study is that SMR performance strongly depends on the reactor type. Existing SMR concepts can be grouped into four main categories:

- Water-cooled reactors, such as Pressurised Water Reactors (PWRs) and Boiling Water Reactors (BWRs);
- High-temperature gas-cooled reactors (HTGRs), typically using helium as coolant;
- Liquid metal fast reactors (LMFRs);
- Molten salt reactors (MSRs).

The reactor technology determines the achievable outlet temperature and the quality of the heat that can be supplied for cogeneration and/or conversion. Table 2.1 summarises typical operating temperature ranges and electrical output of SMR designs.

Table 2.1: Typical operating temperature of existing SMR technologies [27]

Reactor Type	$\mathbf{T}_{Range}$ **[°C]**
PWR	up to 350
LMFR	550–650
MSR	650–800
HTGR	700–1000

However, the average temperatures required during steelmaking are typically above 1000 °C [30]; therefore, even advanced SMRs cannot fully meet the corresponding heat demand. As a result, it is not technically feasible for an SMR to directly supply the process heat needed for these operations without additional high-temperature boosting systems or hybrid solutions.

For this reason, this study investigates an alternative integration pathway: using the SMR primarily as a low-carbon electricity source while exploiting its cogeneration capability to

provide a high-temperature electrolysis technology, namely the Solid Oxide Electrolysis Cell (SOEC) [20].

This configuration employs Solid Oxide Electrolysis Cells (SOECs), operating at temperatures of approximately 800 °C, where steam is electrochemically split into hydrogen and oxygen using oxide ions as charge carriers [20].

2.3. Object of the thesis

After presenting the decarbonization challenge of hard-to-abate sectors, which represent a significant share of global energy-related CO_2 emissions, and after introducing the process configuration and baseline operating conditions of the selected case study, the specific objectives of this thesis can be defined.

The aim of this work is to investigate **the integration of low-carbon energy supply** options into the energy system of the Empresa Siderúrgica del Mutún, with a particular focus on **hydrogen-based steelmaking pathways**. To this end, the objectives of the study are presented:

- To extend the Reference Energy System of the Empresa Siderúrgica del Mutún to explicitly account for Hydrogen demand associated with the DRI process, and to model the corresponding Hydrogen production technologies and energy supply chains required to meet this additional demand.
- To assess the potential reduction in direct CO_2 emissions, the considered configurations are compared using indicators such as total emissions and CO_2 intensity. In particular, hydrogen-based DRI configurations are evaluated against the natural-gas-based baseline case by comparing two hydrogen production technologies, low-temperature electrolysis (PEM) and high-temperature electrolysis (SOEC), together with the corresponding low-carbon energy supply options.
- To assess the technical feasibility and economic viability of alternative technological pathways for hydrogen production, different economic indicators are compared, and a territorial characterization is carried out for the location of the Empresa Siderúrgica del Mutún
- These aspects are then synthesized to identify the strengths, limitations, and critical issues of each option and to determine the most suitable configuration under different conditions.

3 | Materials and Methods

This section presents a concise overview of the model used in this study, with a specific focus on the implementation developed for the analyzed case study. In addition, it aims to illustrate how the model has been applied to the system considered.

3.1. Hypatia framework and model structure

In this study, Hypatia is used as the energy system modelling framework. Hypatia is an open-source software written in Python based on CVXPY for the formulation and solution of optimization problems [38].

The model adopts a bottom-up approach and relies on linear programming to identify the optimal system configuration. Through this approach, Hypatia is able to solve both single-objective and multi-objective optimization problems, aiming to determine optimal solutions based on cost and/or emission criteria.

In this work, a single-objective formulation is adopted to identify the solution that minimizes the Net Present Cost (NPC). To this end, the following objective function is implemented within the software[43]:

$$\begin{aligned} &\text{minimize} && f(x) = [\text{NPC}(x)] \\ &\text{subject to} && \begin{cases} y_i(x) \leq 0 \quad i \in [1, \ldots, m] & m \text{ – inequality constraints} \\ h_l(x) = 0 \quad l \in [1, \ldots, q] & q \text{ – equality constraints} \end{cases} \\ &\text{with} && x = [x_1, x_2, \ldots, x_n] \qquad n \text{ – decision variables} \end{aligned} \tag{3.1}$$

In particular, the Net Present Cost (NPC) is expressed by the following equation [43]:

$$\mathrm{NPC} = \sum_{t=1}^{n} \frac{\sum_j \left(\mathrm{CAPEX}_{j,t} + \mathrm{OPEX}_{j,t} + \mathrm{DecomCost}_{j,t} + \mathrm{Tax}_{j,t} - \mathrm{Sub}_{j,t}\right)}{(1+r)^t} - \sum_j \sum_k \frac{\mathrm{SV}_{j,k}}{(1+r)^n} \tag{3.2}$$

where:

- $CAPEX_t$ represents the capital expenditures incurred at time-step t;
- $OPEX_t$ represents the operation and maintenance expenditures incurred at time-step t;
- r and n denote the discount rate and the total lifetime of the system, respectively;
- $DecomCost_t$ represents decommissioning and dismantling costs incurred at time-step t;
- $Taxes_t$ includes all taxes applied at time-step t, such as carbon taxes or fixed levies applied to specific technologies;
- $Subsidies_t$ represents incentives and support schemes applied at time-step t to specific technologies;
- j indexes the technology (or asset type);
- k indexes the investment decision / installation year (i.e., individual vintages of capacity additions);
- $SV_{j,k}$ represents the salvage value associated with investment k of technology j, evaluated at the end of the modelling horizon and discounted to present value through $(1+r)^n$;

The optimization of the NPC is based on different constraints that have to be respected such as [43]:

$$\begin{aligned} \mathrm{tot\_capacity}_{\mathrm{REN/fossil}} &\leq \mathrm{Max\_TotCap}_{\mathrm{REN/fossil}} \\ \mathrm{new\_capacity}_{\mathrm{REN/fossil}} &\leq \mathrm{Max\_NewCap}_{\mathrm{REN/fossil}} \\ &\vdots \\ \mathrm{Supply}_{\mathrm{REN/fossil}} &\leq \mathrm{tot\_capacity}_{\mathrm{REN/fossil}} \times \mathrm{capacity\_factor}_{\mathrm{REN/fossil}} \end{aligned} \tag{3.3}$$

However, the main constraint of the model is the **energy balance**:

$$Demand = Supply \tag{3.4}$$

which ensures that the system is able to identify the optimal solution while fully satisfying the energy demand.

Under the constraints described above, the model aims to minimize the Net Present Cost through the optimization of the two *decision variables* reported in Table 3.1.

Decision Variables	
`tech_production`	Activity output of each technology, by carrier, by year and timestep
`new_capacity`	New capacity installed of each technology, by year

Table 3.1: Main decision variables of the Hypatia model.

As a consequence, the model combines the optimal decision variables with the input parameters reported in Table 3.2 in order to compute additional outputs, such as the ones summarized in Table 3.3.

Category	**Parameter**	**Description**
Economic	`INV`	Overnight investment cost.
	`V_OM`	Variable operation and maintenance cost.
	`F_OM`	Fixed operation and maintenance cost.
	`Discount_rate`	Discount rate used for the calculation of the Net Present Cost.
	`Interest_rate`	Interest rate applied to investment costs in the CRF formulation.
Performance	`Tech_efficiency`	Energy conversion efficiency.
	`Tech_availability`	Availability factor of the technology over the year.
	`capacity_factor_resource`	Maximum exploitable resource per unit of installed capacity.
	`Residual_capacity`	Existing installed capacity.
Environmental	`Specific_emissions`	Emission intensity of the technology.
	`Emission_capture_efficiency`	Fraction of captured emissions, when applicable.
Scenario-based	`Min/Max_newcap`	Bounds on newly installed capacity.
	`Min/Max_totalcap`	Bounds on total installed capacity.

Table 3.2: Main input parameters of the Hypatia model.

Derived Model Outputs	
`tech_use`	Consumption of each technology, carrier, year and timestep
`tech_cost`	Cost of each technology, by year and cost category
`total_capacity`	Cumulated installed capacity of each technology, by year
`emissions`	Amount of emissions released of each technology, by year

Table 3.3: Derived outputs of the Hypatia model.

While performing these decision-making processes, Hypatia can operate over different time horizons depending on the modelling mode adopted:

- *Operational Mode*: operation at high temporal resolution;
- *Planning Mode*: operation over long-term time horizons.

All the modelling features and characteristics presented in this section are schematically illustrated in Fig. 3.1.

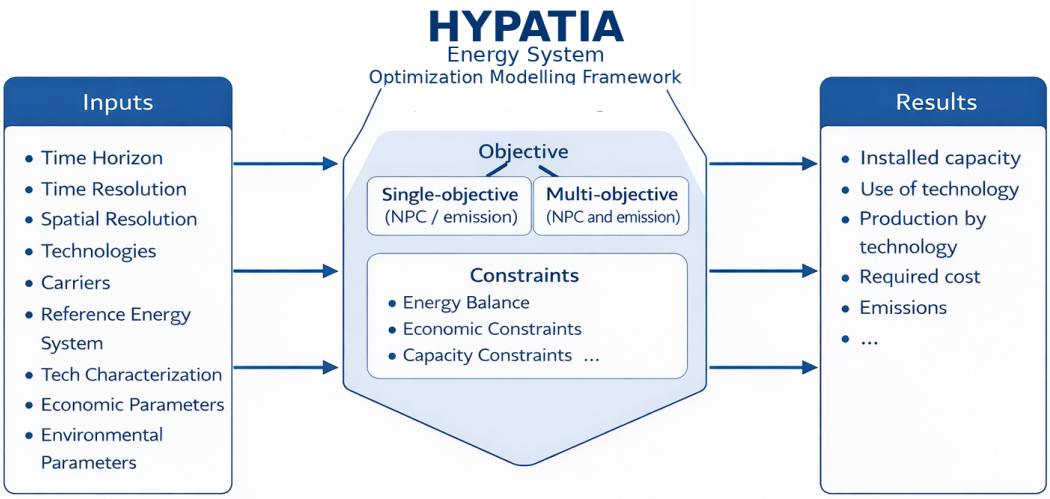

Figure 3.1: Schematic representation of the Hypatia modelling framework, highlighting operational and planning modes.

3.2. Timeseries clustering

As already mentioned in the previous section, the Hypatia software can operate over a long-term time horizon when running in *Planning Mode*. The case study considered in this work aims to analyse the current situation of the system as well as its evolution over the following 25 years[1].

To do so, the model requires as input a number of time steps equal to the total hours of the year for each modelled year. In this case, the time horizon corresponds to 25×8760 time steps. However, handling such a large number of time steps can be computationally demanding, especially when computational resources are limited. For this reason, a time aggregation method is adopted in this work.

It should be noted that clustering-based aggregation methods do not provide a perfect representation of the original time series, and a certain level of approximation must be accepted when applying time series aggregation. However, the relevance of this approximation depends on the decisions derived from the aggregated data.

The selection of representative typical periods must be carried out according to well-defined criteria. For this reason, this study uses the open-source Python package TSAM (Time Series Aggregation Module), developed by Hoffmann and Kotzur [33].

The TSAM package requires as input the number of representative periods, the length of each period, and the aggregation method to be used. The choice of these parameters depend on the case study and must be carefully evaluated.

The following key questions should be taken into consideration:

- Which time-series aggregation method is best suited for the energy system design application?
- What is the minimum number of aggregated time steps to model such a system?
- What is an appropriate period length, typical days or typical weeks?

The objective is to identify the most suitable answers to the questions introduced above. Since no unique or universally optimal solution exists, these choices must be made to the specific characteristics of the considered case study. The methodological decisions adopted in this work are motivated and discussed below:

- **Time-series aggregation method**: Based on the literature review, a medoid-

[1]This time horizon is required to adequately represent the deployment of SMR technology, which is assumed to become available from 2035.

based aggregation method was selected for this study [28]. This approach preserves real temporal profiles and extreme events, which is crucial for the present case study, characterized by high RES penetration and the use of battery storage systems. As a result, it provides a more reliable representation of capacity constraints and cost-optimal investment decisions, while maintaining a reasonable computational burden.

- **Number of aggregated time steps**: For this study, six aggregated time steps were selected. Three of them are computed directly using the TSAM package and represent the three main seasons, which strongly affect solar availability. Following the literature, two extreme periods were added to capture the best and worst days in terms of wind and solar capacity availability [28]. The final time step represents a system shutdown condition, allowing for a clearer assessment of the availability of the different technologies.
- **Length of time steps**: An aggregation period length of 72 hours (three days) was adopted. The 72 hours window is used to capture the battery state of charge evolution across consecutive days and to reduce boundary effects when representative periods are modelled as independent blocks. Similar three-day representative periods have been explicitly assessed in time-series aggregation studies including battery storage [28].

The final outcome of the time aggregation is a representative description of each year in the analysed time horizon, which can be represented as follows:

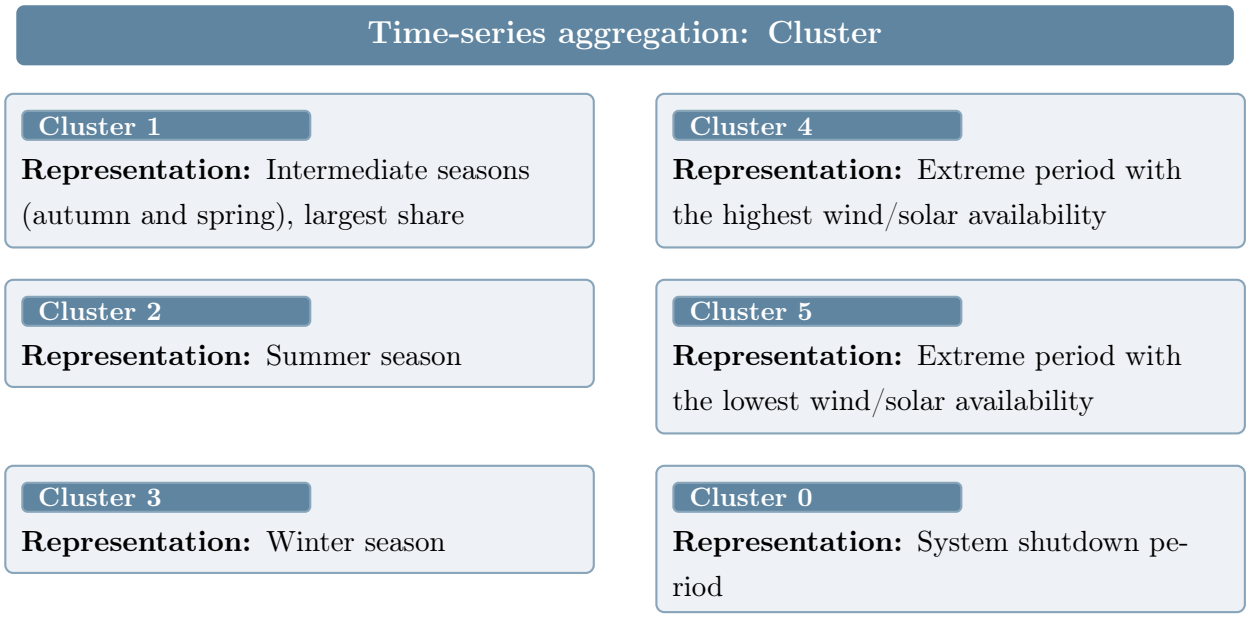

Figure 3.2: Block representation of the adopted time-series aggregation (clusters and weights).

After these decisions, it is important to clarify how the selected typical periods represent the entire year through their associated weights, as provided by TSAM and further adjusted to include the additional clusters required for an adequate representation of the year. As a consequence, the demand profile must also be adapted, particularly to account for the introduction of cluster 6, which is characterized by zero demand and whose contribution must therefore be redistributed across the remaining clusters.

Figure 3.3 illustrates all the steps of the clustering procedure, from the initial input data to the compilation of the model parameters.

TSAM setup (candidate periods)

TSAM splits the 8760-hour time series into candidate periods of 72 hours, i.e. 8760/72 c.p. Each c.p. is a 72×2 matrix containing wind and solar capacity factors (CF_{wind}, CF_{solar}) for 72 timesteps. TSAM clusters these c.p. and identifies representative periods for $K = 3$ clusters.

TSAM outputs: representative periods and weights

TSAM returns 3 representative periods, each consisting of 72 values for CF_{wind} and for CF_{solar}. TSAM provides a weight for each cluster, i.e. how many times that 72-hour period is repeated over the year. The total number of represented hours must satisfy:

$$\sum_{k=1}^{3} w_k \cdot 72 = 8760.$$

Manual integration: extreme periods and shutdown period

Two additional periods are selected manually: the best and the worst period of the year in terms of $CF_{\text{solar/wind}}$, representing clusters 4 and 5. Cluster 6 is created with demand equal to zero to represent the system stop.

Weight adjustment after adding new clusters

After adding clusters 4-6 and their corresponding weights[a], the weights of the original clusters must be updated so that the total represented hours remains 8760:

$$\sum_{k=1}^{6} w_k \cdot 72 = 8760.$$

[a] In this case, the added clusters have weight equal to 1, as it occurs only once per year period.

Time fractions for each cluster

A time fraction is associated with each cluster as:

$$\text{tf}_k = \frac{w_k \cdot 72}{8760}, \qquad \sum_{k=1}^{6} \text{tf}_k = 1$$

Building the model inputs with consistent proportions

All time-dependent inputs must be compiled respecting the cluster time fractions. In particular, demand is assigned at each timestep according to [a]:

$$\text{DEMAND}(t) = \overline{P}\,[\text{kW}] \times 8760 \times \text{tf}(t),$$

[a] The demand of cluster 6 (shutdown period) is redistributed across the remaining timesteps.

Figure 3.3: Workflow used to integrate TSAM representative periods with additional manually selected clusters and to compute consistent time fractions.

Given the considerations above, it is important to evaluate the impact of the adopted year representation and the quality of the time-series aggregation. For this purpose, Fig. 3.4 reports the hourly solar availability[2] over a 72-hour time slice for Clusters 1 to 5. Cluster 0 (shutdown) is not reported, as the demand is assumed to be zero during that period.

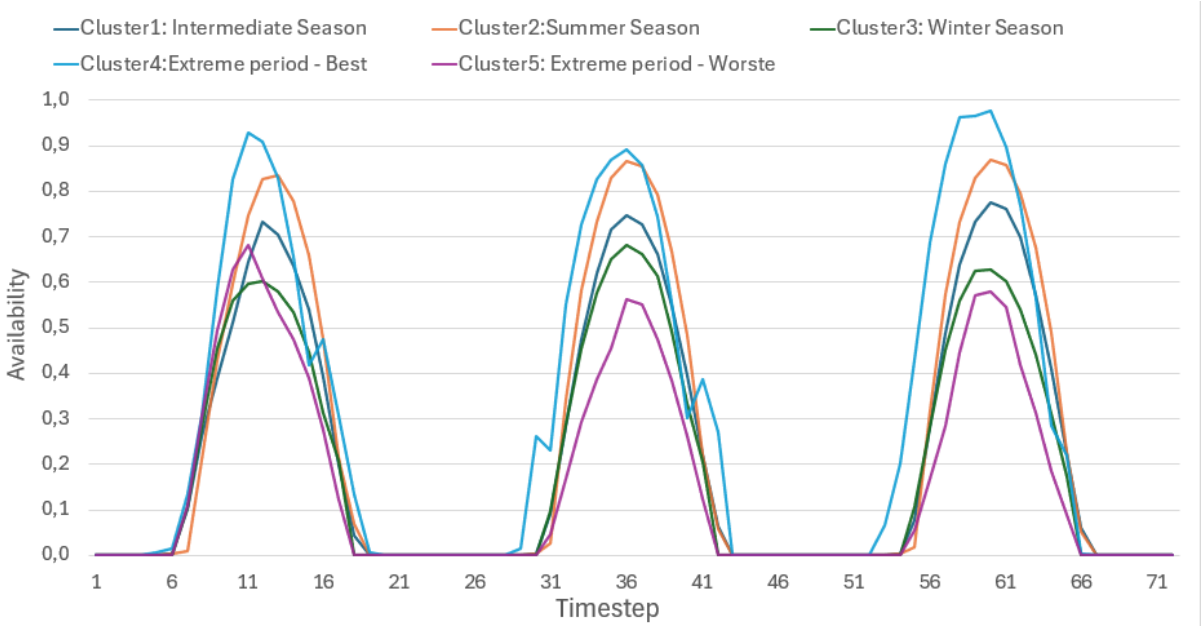

Figure 3.4: Hourly solar availability over the representative 72-hour period for each cluster.

3.3. Modelling of Nuclear Reactor cogeneration

At this stage, it is important to clarify how the SMR's cogeneration capability is represented within the model.

Steam-driven CHP plants can be classified into two main categories: (i) backpressure turbine plants, characterised by a fixed power-to-heat relationship, and (ii) extraction/condensing turbine plants, where heat production is **flexible** and can vary (within technical limits) independently of power output [5].

The second category is adopted in this study and can be represented through a two-dimensional **Feasible Operation Region (FOR)** in the power–heat plane, bounded by:

- a **power-loss** relationship, which captures the decrease in electric output when more useful heat is extracted;

[2]Only solar availability is shown because solar is the only renewable technology considered in this study; wind is not included.

- a **heat-to-power** bound, which limits the maximum share of heat relative to electricity;
- an upper bound on the **maximum useful heat** that can be delivered.

Consistent with this flexible representation, the following linear constraints are considered [5]:

$$\mathrm{P} = \eta_{\mathrm{el}}^{100\%}\,\mathrm{prod}_{\mathrm{CHP}} - \zeta\,\mathrm{Q} \tag{3.5}$$

$$\mathrm{Q} \leq \gamma\,\mathrm{prod}_{\mathrm{CHP}} \tag{3.6}$$

$$\mathrm{Q} \leq \alpha\,\mathrm{P} \tag{3.7}$$

where P denotes the electricity output, Q the useful heat output, and $\mathrm{prod}_{\mathrm{CHP}}$ the upstream cogeneration energy flow from the reactor to the CHP module, the energy available before the electricity/heat split and conversion efficiencies.

In this formulation, Eq. (3.5) represents the power penalty associated with heat extraction (slope ζ), Eq. (3.6) limits the maximum deliverable useful heat through γ, and Eq. (3.7) bounds the heat-to-power ratio through α.

The set of constraints introduced above defines the feasible operating region (FOR) of the SMR in cogeneration mode for this study [25]. The resulting FOR is shown in Fig. 3.5. Table 3.4 summarises the key parameters used to build the CHP representation.

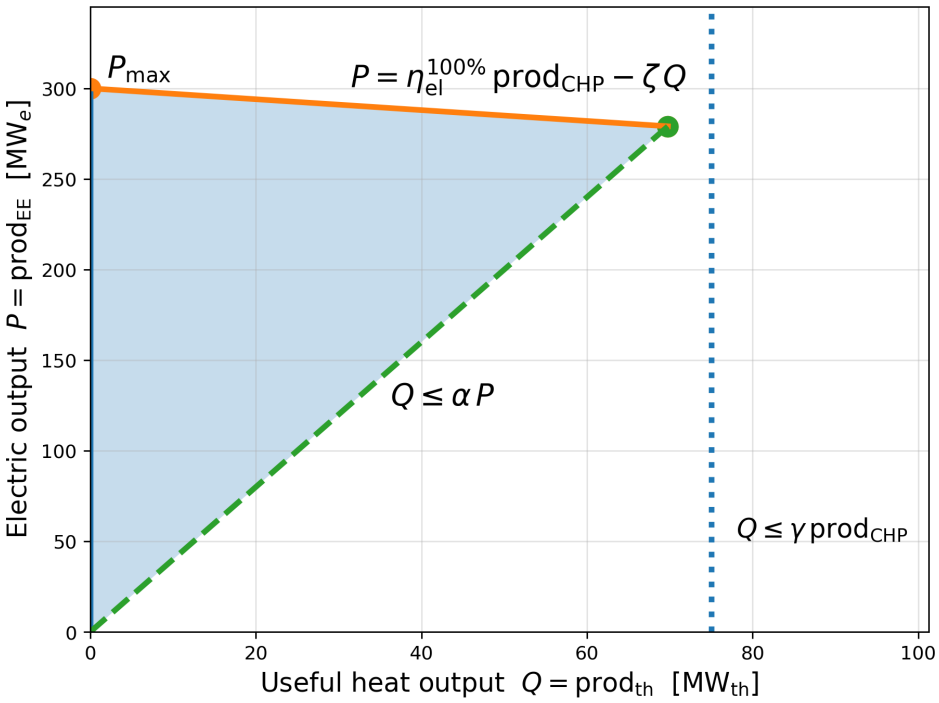

Figure 3.5: Feasible operating region of the SMR CHP unit.

Table 3.4: Key parameters adopted for the SMR CHP model (Hypatia Type 3).

Parameter	**Value**
$P_{\max}$ [MW_e]	300
$\eta_{el}^{100\%}$ [-]	0.40
γ [-]	0.10
ζ [-]	0.30
$\alpha = \gamma/\eta_{el}^{100\%}$ [-]	0.25
$P_{th,reactor}^{nom} = P_{\max}/\eta_{el}^{100\%}$ [MW_{th}]	750

4 | Case Study: Empresa Siderúrgica del Mutún

The *Empresa Siderúrgica del Mutún* (ESM) is located in Puerto Suárez, in the Santa Cruz Department of eastern Bolivia. Located near the border with Brazil, the site is within the region of the El Cerro Mutún iron ore deposit, one of the largest iron ore reserves in the entire world [23].

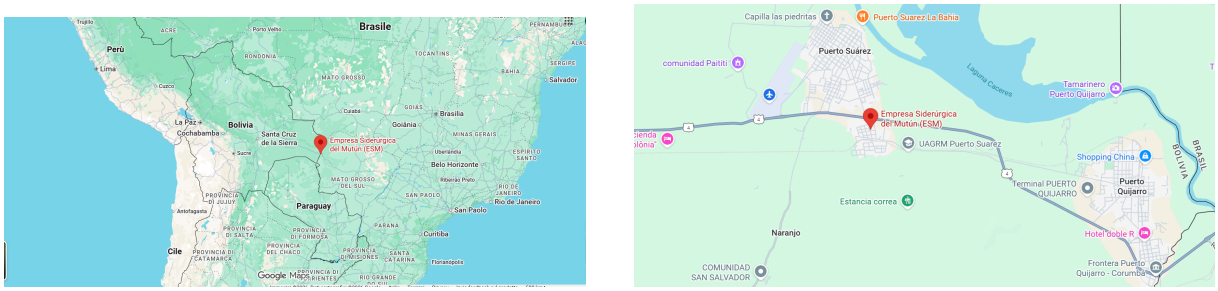

Figure 4.1: Geographical location of the Empresa Siderúrgica del Mutún in Bolivia. Source: Google Maps.

ESM represents Bolivia's first major industrial steelmaking facility. The complex comprises multiple interconnected production units, including iron ore concentration, pelletizing, direct reduced iron (DRI) production, electric arc furnace (EAF) steelmaking, and rolling mills [23]. This process configuration closely reflects the general steelmaking route discussed in the previous sections.

4.1. Territorial resources: solar, wind and water

The *Empresa Siderúrgica del Mutún* is located in the eastern lowlands of Bolivia, within the broader Gran Pantanal system. The Pantanal is a large wetland region characterised by strong seasonality (wet and dry seasons) and significant interannual variability, which can affect both energy resources and the availability of water for industrial uses [40].

4.1.1. Solar resource

Solar energy is the primary renewable resource considered in this study. Figure 4.2 reports the long-term average Global Horizontal Irradiation (GHI) in Bolivia. The national pattern is strongly influenced by topography: the highest irradiation levels occur in the western region, while the eastern lowlands show moderate-to-good values. The Mutún/Puerto Suárez area falls within a favourable area for photovoltaic (PV) generation [14].

However, the Pantanal's wet season can increase cloud cover and reduce solar availability, implying a seasonal variability in PV output.

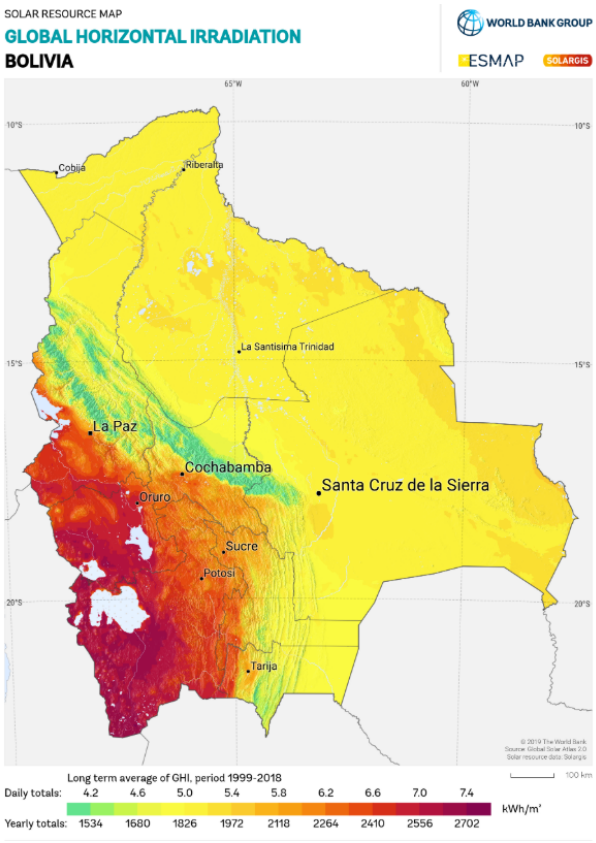

Figure 4.2: Long-term average Global Horizontal Irradiation (GHI) in Bolivia [14].

4.1.2. Wind resource

Wind availability in Bolivia is highly heterogeneous and strongly influenced by regional circulation patterns. A preliminary screening can be obtained from the Global Wind Atlas map of long-term mean wind speed at 100 m (Fig. 4.3). The map highlights a clear spatial contrast: higher wind speeds are mainly associated with specific regions, while the eastern lowlands appear generally characterised by lower-to-moderate wind speeds [15].

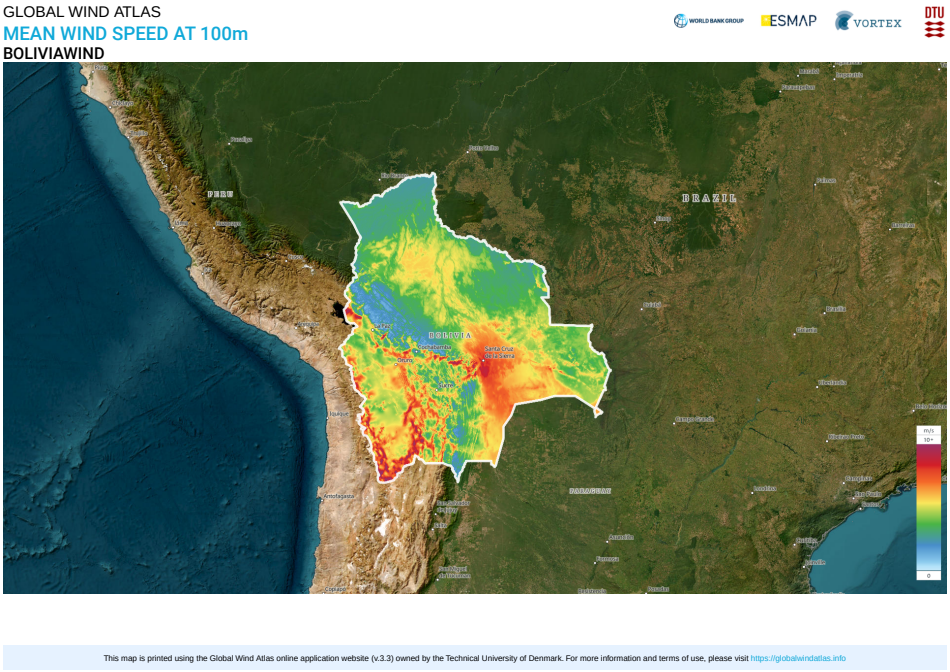

Figure 4.3: Long-term mean wind speed at 100 m in Bolivia. Source: Global Wind Atlas v3.3 (DTU/World Bank/ESMAP).

4.1.3. Water resources

The site is situated in the vicinity of Laguna Cáceres and is connected to the Paraguay-Paraná waterway through the Tamengo Canal. This hydrological setting is relevant for two reasons [40]:

- It provides strategic access to inland navigation routes.
- It highlights the importance of accounting for local water availability and seasonal constraints when discussing the feasibility of water-intensive technologies.

From a territorial perspective, the study area lies within the broader Gran Pantanal system. As a result, water availability cannot be described solely by the presence of lakes and river corridors: it is also shaped by seasonal water-level fluctuations, flood pulses, and periods of reduced availability during dry spells [26].

4.2. Plant Characterization

The plant under study currently relies on natural gas-based technologies to meet both the electrical and heat demands of the facility. It is based on internal combustion engines to meet the electricity demand, and on gas-fired burners to supply the heat requirements of

the plant. Therefore, the facility is entirely dependent on natural gas for its operation.

As a consequence, the Reference Energy System in its current configuration presents a limited number of technologies, each specifically dedicated to meeting either the electricity demand or the heat demand of the plant.

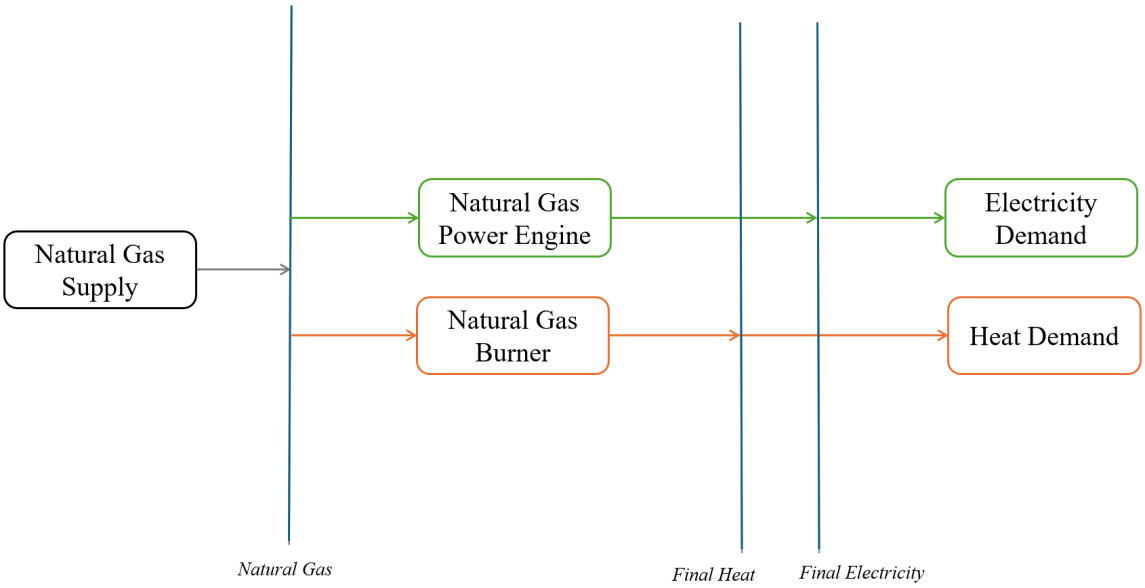

Figure 4.4: Current Reference Energy System of the Plant

Having established the plant's current Reference Energy System, the following section introduces the dataset and key assumptions used to characterise the baseline operating conditions. The assessment is based on a combination of primary data provided by the *Empresa Siderúrgica del Mutún* and additional estimations developed within the scope of this study. The initial values of electricity, thermal energy, and water consumption are directly sourced from technical documentation supplied by the Bolivian plant and represent the reference operating conditions of the facility.

4.2.1. Plant energy demand: electricity and heat

Table 4.1 reports the average hourly electrical power required by each process, assuming continuous and steady-state operation of the plant. The demand is reported for three distinct development steps, which represent the planned evolution of the plant and illustrate the progressive increase in electricity requirements during the periods 2025–2029, 2030–2035, and 2036–2040.

Table 4.1: Steel plant electrical demand evolution by process and development step

	Average Hourly Electrical Power Demand in MW		
Process	Step 1: 2025–2029	Step 2: 2030–2035	Step 3: 2036–2040
Concentration	5.7	17.1	39.9
Pelletizing	2.7	5.4	16.2
DRI	3.9	7.7	23.1
Steel Mill	48.2	96.5	289.4
Rolling Mill	7.8	15.5	46.6
Auxiliary Facilities	7.0	13.7	41.4
TOTAL	75.3	155.9	456.6

The reported values should be interpreted by considering that the production level associated with the first development step corresponds to an annual steel output of 194 000 ton/year.

Based on the evolution of electrical demand across the three development steps, the corresponding increase in annual steel production was estimated from Step 1 to Step 2 and subsequently to Step 3. Assuming a proportional relationship between average electrical power and production rate, the following expression was adopted:

$$Q_{\text{step2}} = \frac{P_{\text{avg, step2}}}{P_{\text{avg, step1}}} \times Q_{\text{step1}}$$

This resulted in an estimated production of approximately 401 655 ton/year for Step 2 and 1 176 367 ton/year for Step 3.

These calculations are valid under the assumption that the specific electrical energy intensity [MWh/ton] remains constant across the three development steps. This assumption is considered reasonable provided that the same technology, efficiency levels, and operational practices are maintained throughout the plant evolution [22].

The Bolivian technical documentation also provides detailed information on the thermal energy requirements of the steelmaking facility. Each process is characterized by a specific thermal demand and a corresponding maximum operating temperature, as summarized in Table 4.2. Unlike the electrical data, thermal demands are reported without distinction between development steps.

Table 4.2: Thermal demand of the steelmaking facility

Process	**Power [MW_{th}]**	**Max Temperature [°C]**
Concentration	0.00	0
Pelletizing	24.86	1350
DRI	93.23	1100
Steel Mill	20.28	1640
Rolling Mill	16.99	1150

To evaluate the evolution of thermal energy demand as a consequence of the increase in steel production, the total thermal load was decomposed into two contributions: a base load, assumed to be independent of production, and a variable load scaling with output. A uniform base-load coefficient of $f = 0.25$ was assumed for all process units [16].

$$P_{\text{th, step2}} = f\, P_{\text{th, step1}} + (1 - f)\, P_{\text{th, step1}} \left(\frac{Q_{\text{step2}}}{Q_{\text{step1}}} \right)$$

$$P_{\text{th, step3}} = f\, P_{\text{th, step1}} + (1 - f)\, P_{\text{th, step1}} \left(\frac{Q_{\text{step3}}}{Q_{\text{step1}}} \right)$$

The resulting thermal power requirements for each process and development step are summarized in Table 4.3.

Table 4.3: Steel plant thermal demand evolution by process and development step

	Average Hourly Thermal Power Demand in MW_{th}		
Process	Step 1: 2025–2029	Step 2: 2030–2035	Step 3: 2036–2040
Pelletizing	24.86	44.8	119.3
DRI	93.23	168.1	447.3
Steel Mill	20.28	36.6	97.3
Rolling Mill	16.99	30.6	81.5
TOTAL	155.36	280.1	745.4

Electricity Load Profile (Hourly Resolution)

For completeness, the hourly electrical load profile provided by the *Empresa Siderúrgica del Mutún* is also considered. The profile is expressed in terms of electrical power [kW] for

each hour of a representative day and describes the instantaneous power demand of the plant over time. This information enables the analysis of short-term demand variations, highlighting potential differences between daytime and nighttime operation.

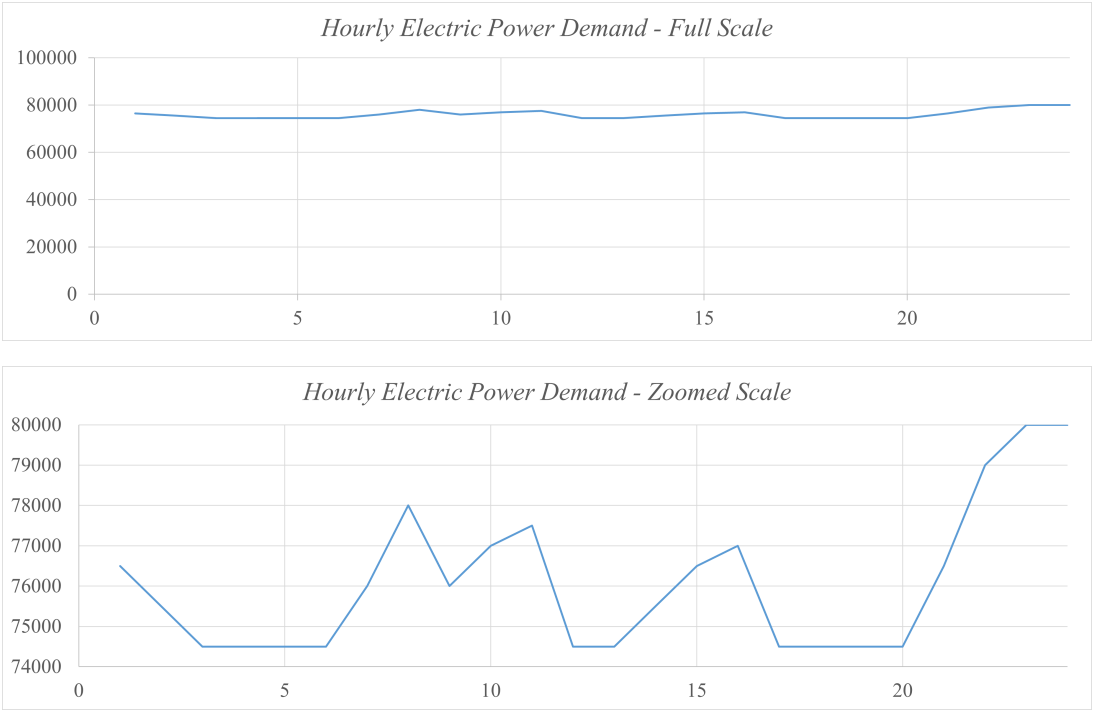

Figure 4.5: Hourly electrical power demand of the steel plant. The upper panel shows the full operating range, while the lower panel provides a zoomed-in view highlighting the small fluctuations.

The analysis of the profile shows that the electrical power demand varies between approximately 74.5 MW and 80 MW during the considered day. This corresponds to a fluctuation slightly above 5 MW, equal to about 6% of the average load. As a result, the electrical demand of the facility can be considered relatively stable over time, with no pronounced peaks or abrupt load drops.

4.2.2. Water Consumptions and Utilities

The Bolivian technical documentation also includes data on the water consumption of the steelmaking facility. In industrial steel plants, water is primarily used as a cooling medium, while its direct use as a process input is limited [12].

Table 4.4: Water consumption per process phase

Process	**Water consumption [m^3/h]**
Concentration	76
Pelletizing	17
DRI	40
Steel Mill	180
Rolling Mill	45
Other	8
Domestic water	6.25
Water treatment	20

This water consumption is aligned with the water demand of a steel plant of this scale [12].

In particular, the water supply of the *Empresa Siderúrgica del Mutún* relies on an aqueduct to convey water from the Paraguay River across the Otuquis National Park and Integrated Management Natural Area (ANMI Otuquis), a protected area within the Pantanal. According to a parliamentary inspection report, a washing plant has been built on site, water would be sourced from the San Juan River and the Paraguay River. [2].

4.3. Scenario Selection

After describing the state of the art of Empresa Siderúrgica del Mutún, it is important to underline the possible pathways for the company to introduce hydrogen. The different scenarios considered in this study are defined to identify how demand is met relative to the baseline case. Each scenario specifies the set of technologies and low-carbon supply options adopted.

- Baseline scenario
- Renewable Energy scenario
- SMR scenario
- Blended scenario

The qualitative description of the scenarios analyzed is complemented by Figure 4.6, which summarize the technological evolution in the different development steps.

	Step 1: 2025–2030	Step 2: 2030–2035	Step 3: 2035–2040
Baseline	NG-based DRI	NG-based DRI (capacity expansion only)	NG-based DRI (capacity expansion only)
RES–H_2 (2030)	NG-based DRI	H_2-based DRI: PEM + RES + Battery	H_2-based DRI: PEM + RES + Battery
SMR–H_2 (2035)	NG-based DRI	NG-based DRI (capacity expansion only)	H_2-based DRI: SMR + SOEC
Blended	NG-based DRI	H_2-based DRI: PEM + RES + Battery	H_2-based DRI: SMR + SOEC + Battery

Figure 4.6: Scenario pathways across development steps (technology configuration adopted in each time window).

It is important to underline the main difference between the baseline configuration and the additional configuration that includes hydrogen demand.

- From the baseline case to the other scenarios, the only change occurs in two specific stages of the steelmaking process: the DRI–EAF route, which in the baseline case is based on natural gas (NG–DRI–EAF), while in the other scenarios it is based on hydrogen (H_2–DRI–EAF). This configuration remains unchanged regardless of whether RES or SMR is adopted.
- All the other stages of the facility are assumed to remain constant in all configurations.
- The other important difference concerns the introduction of a new technology, which is used both for electricity production to supply the hydrogen demand and to meet the electricity demand of the plant.

In this sense, the analysis considers the steelmaking process as a whole; however, the differences among the cases analyzed are essentially limited to the aspects outlined above.

4.4. Reference Energy System

The Reference Energy System of the plant must be modified by introducing water electrolysis technology, together with the corresponding energy supply options. The updated RES are shown in the figures below.

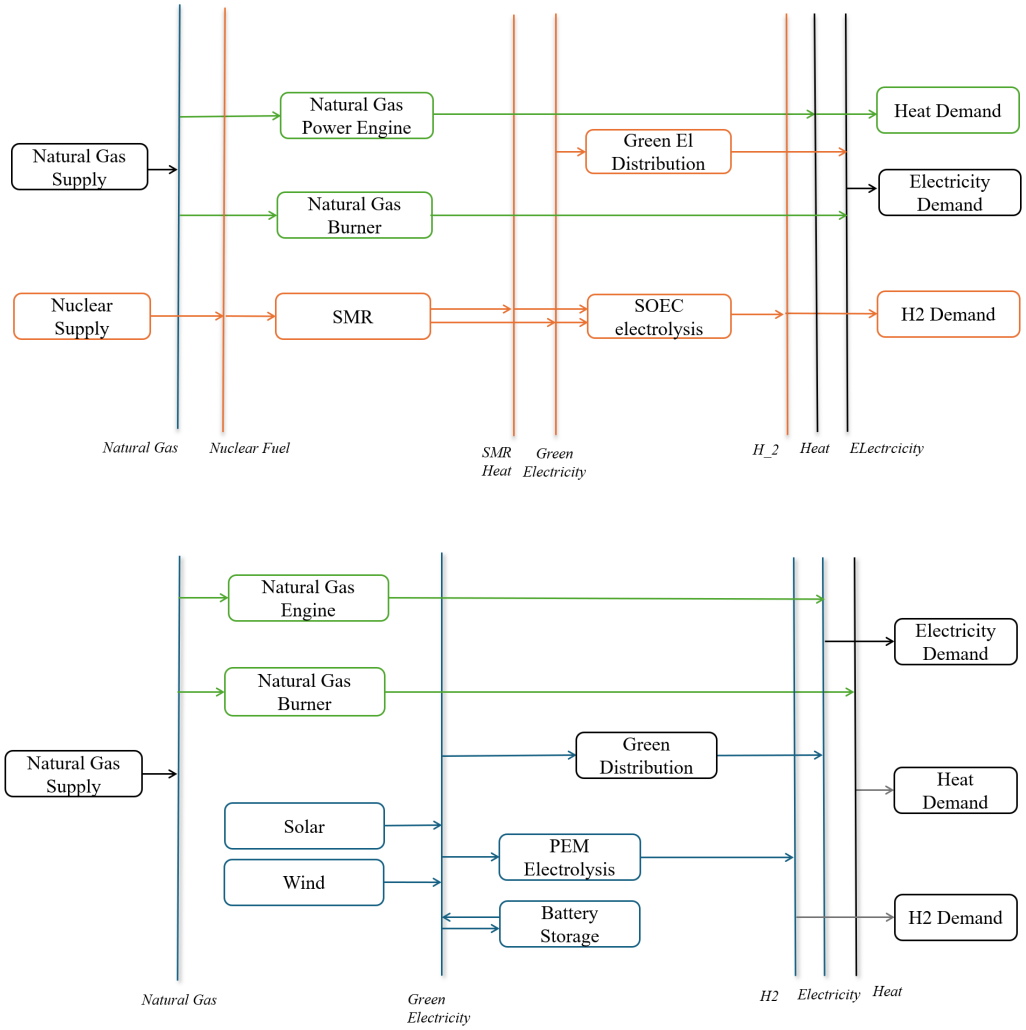

Figure 4.7: Updated reference energy systems for hydrogen production

As shown by the two reference energy systems, both the SMR-based and renewable-based configurations affect the hydrogen production pathway and the electricity supply branch, since electricity is required both for electrolysis and for meeting the plant's electrical demand. Neither the SMR nor the renewable configurations are considered suitable to satisfy the thermal energy demand of the heat branch. This is due to the fact that renewable energy sources are not able to provide the high-temperature heat required for steelmaking [11]. Moreover, according to literature, even the most advanced Small Modular Reactors are currently unable to deliver heat at the temperature levels required by the steelmaking process [25].

4.5. H_2 Demand for DRI Conversion

This section quantifies the additional hydrogen demand required by the plant and the associated adjustments to electricity consumption needed to accommodate the introduction of hydrogen-based technologies.

The hydrogen demand must be accurately estimated to ensure the target steel production at each development stage. In this study, a partial substitution of 30% of the reforming gas with hydrogen is assumed. As discussed in the previous chapter, a full substitution would require substantial plant modifications and is therefore not considered.

According to literature sources [36], the theoretical hydrogen consumption for H_2-based direct reduced iron (DRI) production is approximately 50 kg H_2/t_{steel}, assuming ideal reaction efficiency in the shaft furnace. Under real industrial operating conditions, this value may increase up to about 60 kg H_2/t_{steel}. For the purposes of this analysis, a conservative value of 55 kg H_2/t_{steel} is adopted.

The hydrogen demand is also influenced by the scrap-to-iron ratio in the Electric Arc Furnace (EAF). Higher scrap shares reduce the required amount of sponge iron per tonne of steel. However, according to the official documentation of the Bolivian project, both EAF units are assumed to operate with zero scrap input in the initial configuration [23]. As a result, the full sponge iron input per tonne of crude steel is required.

Given a target steel production of 194,000 t/year for the *Empresa Siderúrgica del Mutún*, the corresponding hydrogen demand, assuming a 30% substitution of the reforming gas, can be calculated as:

$$\dot{V}_{H_2} = 55 \frac{kg_{H_2}}{t_{steel}} \times 194{,}000 \frac{t_{steel}}{year} \times 0,3 = 3{,}201{,}000 \frac{kg_{H_2}}{year} \approx 3{,}201 \frac{t_{H_2}}{year}$$

The projected increases in steel production throughout the development phases are known from the previous analysis. Based on these values, the corresponding hydrogen demand for each development step is calculated and reported in Table **??**.

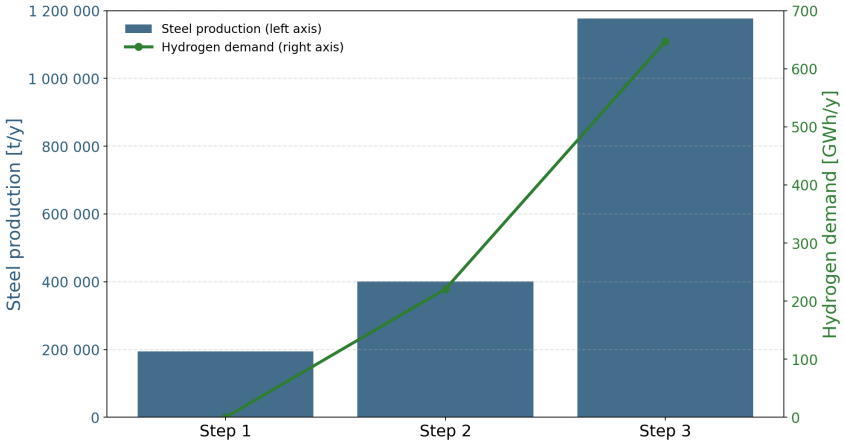

Step	Steel (t/y)	H_2 (t/y)
Step 1	194,000	0
Step 2	401,655	6,627
Step 3	1,176,367	19,410

Figure 4.8: Hydrogen demand and steel production by development step (30% H_2 in DRI).

5 | Results

In this chapter, the results of the different scenarios are presented and discussed. The main objective is to compare the considered alternatives and identify the most suitable solution for the *Empresa Siderúrgica del Mutún*.

To support the comparison, each scenario is assessed through a set of key indicators, which are reported and discussed throughout the chapter.

Figure 5.1 shows the installed capacity in the third development step, the stage in which the full portfolio of technologies considered in each scenario is assumed to be available.

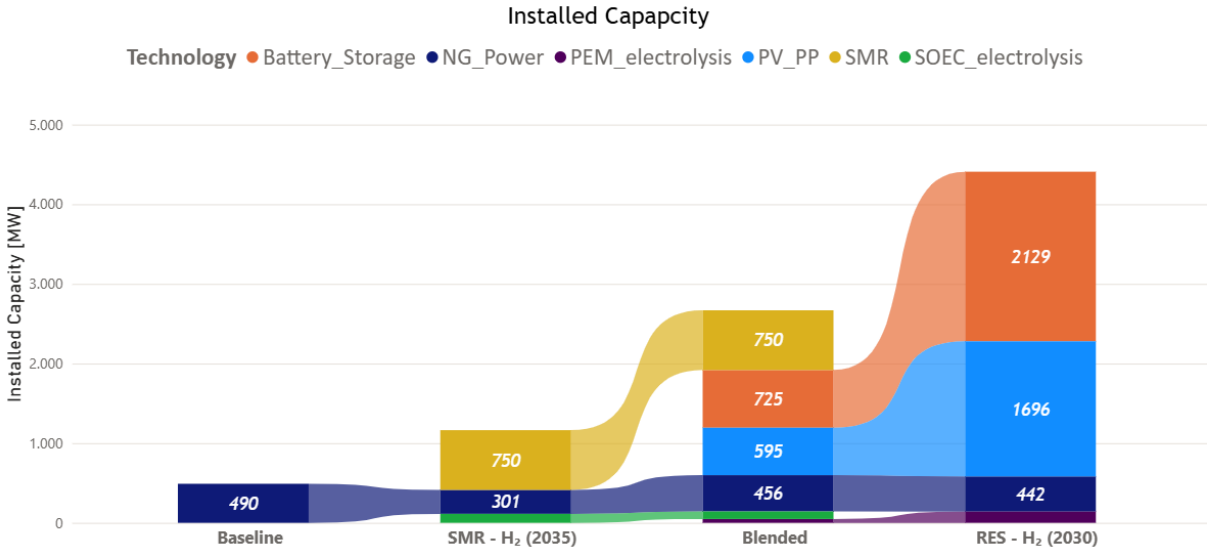

Figure 5.1: Installed capacity in the third development step

Differences in the installed capacity mix directly translate into different requirements for natural gas (NG) power capacity across scenarios. In particular, the reduction in NG installed power with respect to the Baseline case is:

$$\Delta \mathrm{NGP}^{\mathrm{Base–Blended}} = 34 \text{ MW} \quad \Delta \mathrm{NGP}^{\mathrm{Base–RES}} = 48 \text{ MW} \quad \Delta \mathrm{NG}_{\mathrm{P}}^{\mathrm{Base–SMR}} = 189 \text{ MW} \tag{5.1}$$

Beyond installed capacity, it is also important to analyse capacity factors across development steps, as they provide insight into the actual utilisation level of each technology and its operational role within the system.

Table 5.1: NG_Power capacity factors by development step for the analysed scenarios.

Step	**Baseline**	**Blended**	**SMR–H_2 (2035)**	**RES–H_2 (2030)**
Step 1	79.43%	79.03%	79.03%	79.03%
Step 2	100.00%	62.06%	98.59%	64.95%
Step 3	100.00%	66.03%	97.72%	64.95%

The results highlight that the internal combustion engines (ICEs), already installed at the *Empresa Siderúrgica del Mutún* and therefore modeled as *existing capacity*, remain operationally relevant in all scenarios. In the Baseline case, their capacity factor reaches 100% in Steps 2 and 3, indicating continuous operation to meet demand. In scenarios with higher renewable and/or hydrogen penetration (Blended and RES-H_2), the capacity factor decreases consistent with a gradual shift towards balancing and reserve operation. In the SMR-H_2 case, the capacity factor remains high also in the final step, reflecting the strong reliance on NG-based electricity generation and the role of gas-fired units in ensuring system operability.

Additionally, the overall breakdown of energy sources used for electricity and hydrogen production over the 2025-2040 period is illustrated through Sankey diagrams. This representation highlights how the relative shares change across scenarios as a function of the introduced technologies, their utilisation (capacity factors), and their commissioning year.

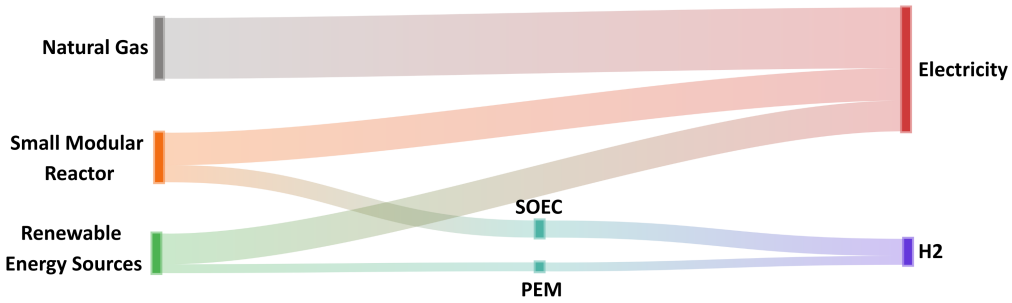

(a) Blended Case

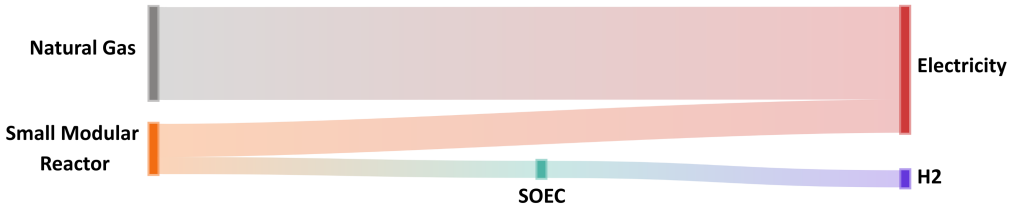

(b) SMR–H_2 (2035)

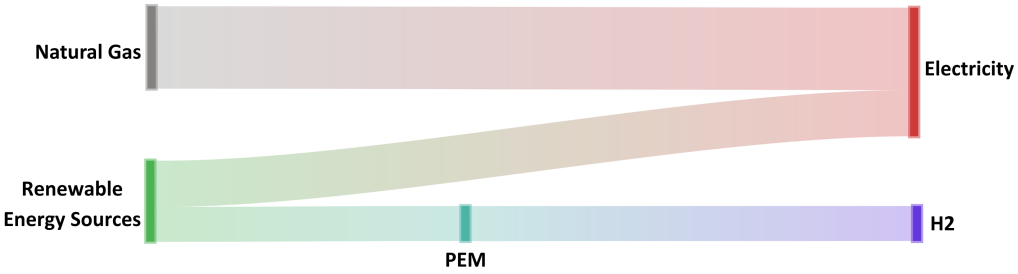

(c) RES–H_2 (2030)

Figure 5.2: Normalized Sankey diagrams (shares, %) showing the breakdown of primary energy inputs to electricity and hydrogen production over 2025–2040 for the three hydrogen scenarios. In each diagram, all flows are expressed as fractions of the total energy input to the electricity+H_2 supply chain, hence the incoming flows sum to 100%.

Flows are expressed as shares (%) and normalized separately for electricity and hydrogen totals, so that each set of incoming flows sums to 100%.

Consistently with the later introduction of SMRs, the SMR-H_2 scenario exhibits the highest natural gas share in electricity generation.

5.1. Environmental impact analysis

Across the different configurations of the scenarios, the introduction of H_2 into the steel-making facility is expected to reduce CO_2 emissions throughout the development steps. The magnitude of this reduction depends on the installed capacities and on the resulting utilization of the available technologies.

In this study, electricity from renewable sources and electricity supplied by Small Modular Reactors are modeled with zero *direct* CO_2 emissions. Additionally, replacing natural gas with hydrogen reduces the overall CO_2 emissions, consistently with the reduction reactions associated with the different DRI pathways.

Natural gas-based DRI (CO/H_2 reducing gas)

$$Fe_2O_3 + 3CO \rightarrow 2Fe + 3CO_2 \tag{5.2}$$

$$Fe_2O_3 + 3H_2 \rightarrow 2Fe + 3H_2O \tag{5.3}$$

H_2-DRI (pure hydrogen reducing gas)

$$Fe_2O_3 + 3H_2 \rightarrow 2Fe + 3H_2O \tag{5.4}$$

This behaviour is reflected in Fig. 5.3, which reports the CO_2 emissions per ton of steel produced for the four scenarios. The indicator is computed as:

$$I_{CO_2,\text{steel}} = \frac{E_{CO_2}}{m_{\text{steel}}} \qquad \left[\frac{\text{tCO}_2}{\text{t}_{\text{steel}}}\right] \tag{5.5}$$

where m_{steel} denotes the steel production (consistent with the time basis used for E_{CO_2}).

Results are reported for one representative year of each development step, since demand and production are assumed constant within each step.

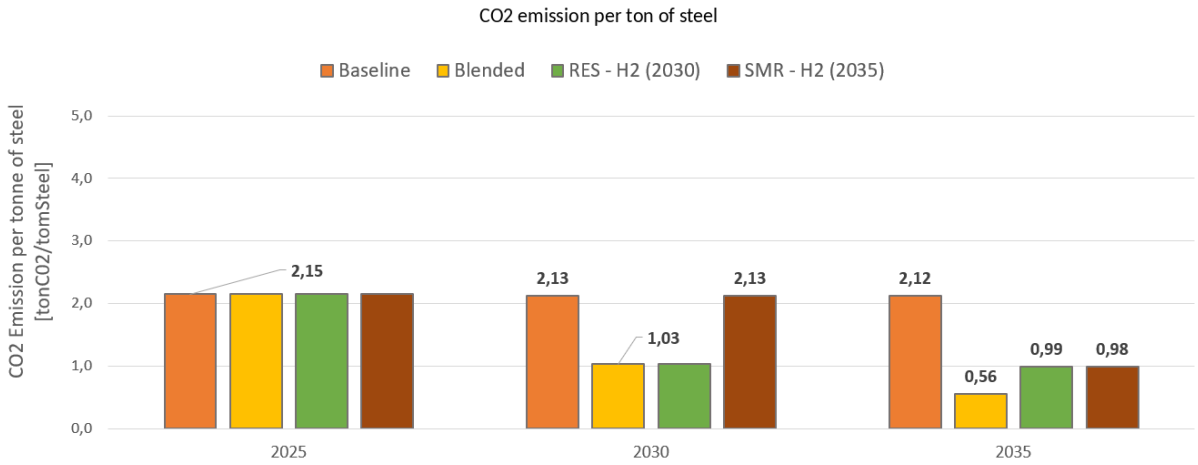

Figure 5.3: CO_2 emissions per ton of steel produced.

The different choices implemented across the four scenarios are clearly reflected in Fig. 5.3. The Baseline scenario exhibits the highest CO_2 emissions; by the third development step, its emissions are nearly twice those of the hydrogen-based cases. Conversely, the three hydrogen-based scenarios show comparable emission levels, with the Blended case achieving the lowest values.

To highlight the effectiveness of each pathway, Fig. 5.4 reports the percentage reduction in total CO_2 emissions relative to the Baseline scenario:

$$\Delta_{CO_2} = \frac{E_{CO_2,\text{baseline}} - E_{CO_2,\text{scenario}}}{E_{CO_2,\text{baseline}}} \cdot 100 \qquad [\%] \tag{5.6}$$

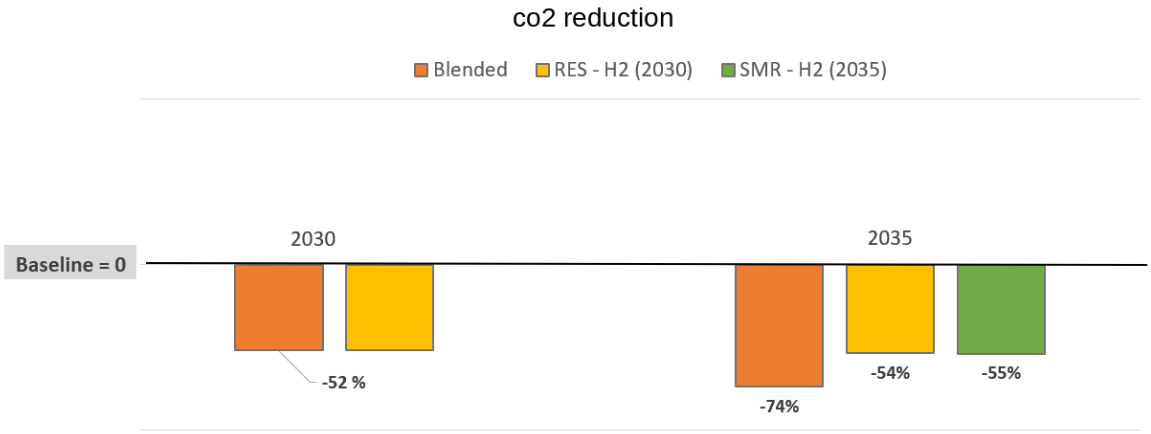

Figure 5.4: Percentage reduction in total CO_2 emissions across scenarios relative to the Baseline case.

In general, hydrogen-enhanced emission reduction is not simply an energy-mixing effect, but mainly a structural consequence of shifting the DRI reducing agent from CO to H_2, thus suppressing intrinsic CO_2 formation at the reactor level. The magnitude of the benefit is therefore primarily driven by the utilization of the hydrogen supply chain, and not only by installed capacities.

5.2. Economic comparison

To better understand the differences among the scenarios, it is also necessary to perform a cost analysis and compare the alternative pathways.

A suitable indicator providing an overall economic picture is the Net Present Cost (NPC), computed by the optimization model as described in the methodology section, over the period 2025–2050 for each scenario.

Figure 5.5 reports the Net Present Cost (NPC) normalized by the total steel production over the analysis horizon, expressed in $/t_steel, for each scenario.

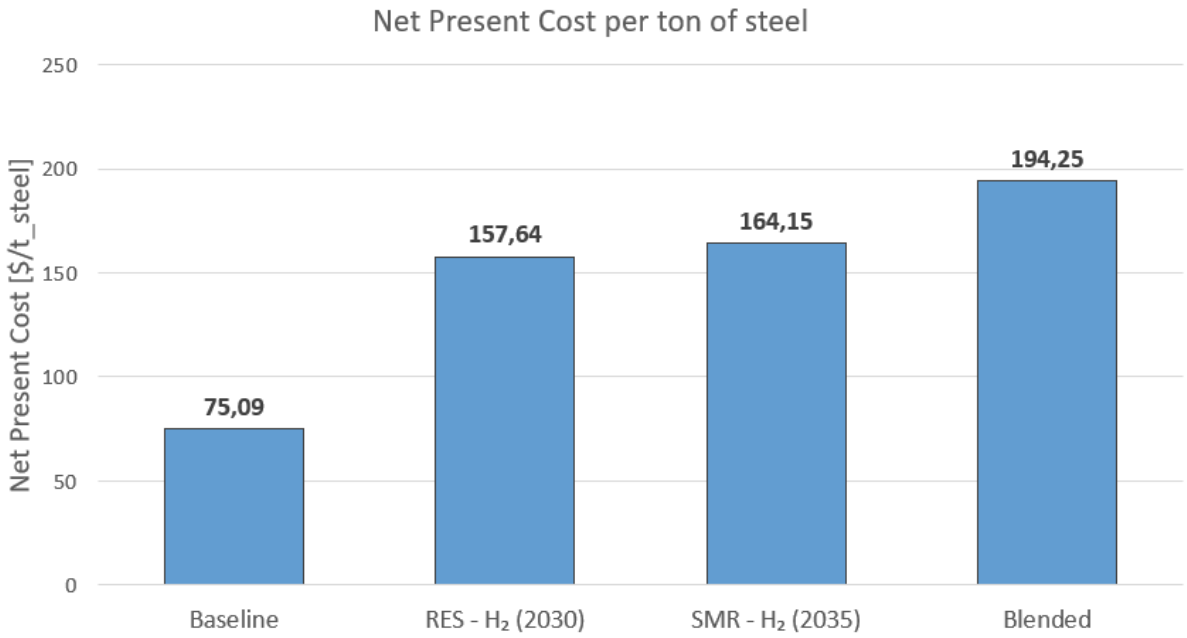

Figure 5.5: Net Present Cost (NPC) normalized by the total steel production over the analysis horizon ($/t_steel) for each scenario. Higher values indicate scenarios with higher cost per ton of steel.

All configurations that include hydrogen production exhibit a higher NPC than the Baseline. This increase is mainly driven by the additional demand for hydrogen, which requires the deployment of new hydrogen production technologies and the associated supply infrastructure.

The difference in NPC between the SMR–H_2 and RES–H_2 scenarios is relatively small. This can be explained by the different cost structures of the electrolysis technologies adopted (SOEC and PEM), whose investment costs evolve over time.

To facilitate comparison across pathways, the cost-effectiveness of decarbonization is quantified through the cost of avoided CO_2, which combines the additional system cost (NPC) with the corresponding emissions reduction relative to the Baseline. Building on the emissions results discussed in the previous section, the cost of avoided CO_2 is computed as:

$$C_{\text{avoid}} = \frac{\text{NPC}_i - \text{NPC}_{\text{base}}}{E_{\text{CO}_2,\text{base}} - E_{\text{CO}_2,i}} \qquad \left[\frac{\$}{\text{tCO}_2}\right] \tag{5.7}$$

where i denotes the scenario being compared against the Baseline. The results are reported in Fig. 5.6.

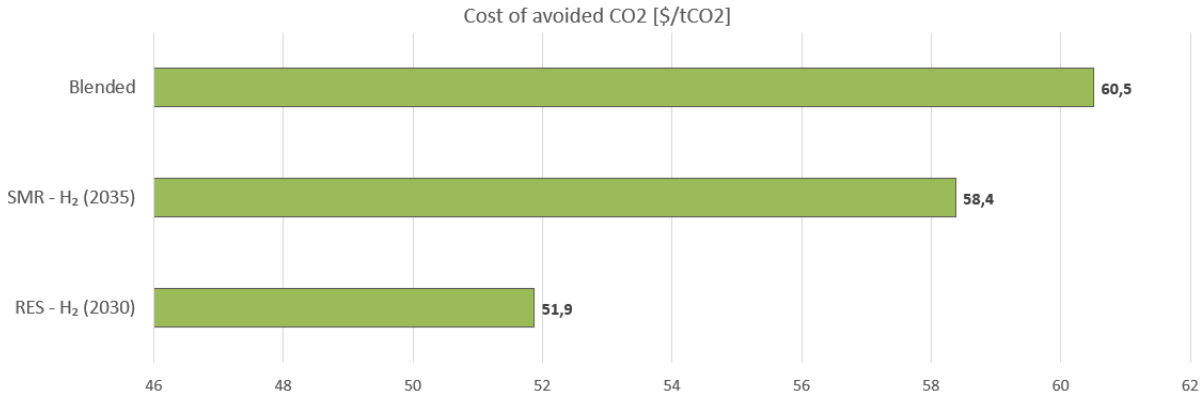

Figure 5.6: Cost of avoided CO_2.

The higher costs associated with hydrogen-based configurations could be partially offset by policy support mechanisms such as carbon pricing, contracts for difference, or carbon credits, which can monetise the avoided CO_2 and therefore reduce the effective cost gap relative to the Baseline. This aspect is discussed in more detail in the following section.

5.3. Carbon credits as a potential pathway

After presenting the emission reduction and cost associated to the four possible pathways for the Bolivian plant it is also important to describe the situation of this country in therm of carbon pricing.

In other countries of Latin America, explicit carbon pricing has taken the form of carbon taxes, with several countries implementing national schemes since the mid-2010s. Recent regional assessments highlight Mexico, Chile, Colombia, Argentina, and Uruguay among the countries that have adopted carbon taxation frameworks, differing in tax base (upstream fuel-based vs. downstream installation-based), coverage, and the possibility of using offsets in some cases. [9]

In contrast, Bolivia is not currently characterized by an operational national carbon tax in the same regional overviews. Instead, recent policy signals suggest a shift toward the development of carbon crediting instruments and market-based climate finance. In particular, reporting indicates that Bolivia expects to obtain sovereign carbon credits, reflecting a marked change in direction toward carbon markets [8].

Looking ahead, a plausible pathway for Bolivia is an increased reliance on carbon crediting mechanisms as a channel to attract climate finance, rather than adopting an explicit carbon tax. Carbon credits are tradable units that represent a verified reduction or removal of

greenhouse-gas emissions, typically expressed as 1 credit = 1 tCO_2e. In practice, a project (e.g., fuel switching, energy efficiency, renewable generation) quantifies its emission reductions against an agreed baseline, and an independent third party verifies monitoring data before credits are issued. Credits can then be sold to buyers (companies or institutions) to support voluntary climate claims or to meet compliance obligations under emerging market frameworks. The economic value of credits is obtained by multiplying the number of issued credits (tCO_2) by a market price (USD/tCO_2), which varies widely depending on credit type, project quality, and market conditions.

Table 5.2: Carbon credit price assumptions used for scenario analysis (voluntary carbon market). [6]

Scenario	Price [USD/tCO_2e]
Low	4.76
Medium	6.97
High	11.80

Assuming that one carbon credit corresponds to one ton of verified CO_2 reduction (1 credit = 1 tCO_2), the annual revenue from carbon credits in year y under scenario s is calculated as:

$$R_{y,s} = \Delta E_{y,s}\, P, \tag{5.8}$$

where $R_{y,s}$ is the carbon credit revenue [USD/ year], $\Delta E_{y,s}$ is the CO emissions $_2$ avoided with respect to the Baseline [tCO_2/ year], and P is the assumed carbon credit price [USD/tCO_2].

In the following, the *Medium* carbon price of $P = 6.97$ USD/tCO_2 is adopted.

To compare carbon-credit revenues with system costs in a consistent manner, revenues are discounted to present value using the same discount rate adopted for the calculation of NPC. The present value of carbon-credit revenues for scenario s is:

$$\mathrm{PV}^{\mathrm{CC}} = \sum_{y=2025}^{2040} \frac{R_{y,s}}{(1+r)^{(y-2025)}} = \sum_{y=2025}^{2040} \frac{\Delta E_{y,s}\, P}{(1+r)^{(y-2025)}}. \tag{5.9}$$

Carbon credits reduce the cost of each scenario by providing an additional revenue stream that can be accounted for in the economic balance. When costs are expressed per unit of product, the credit-adjusted Net Present Cost is defined as:

$$\mathrm{NPC}^{\mathrm{net}}_{\mathrm{steel}} = \mathrm{NPC}_{\mathrm{steel}} - \mathrm{PV}^{\mathrm{CC}}_{\mathrm{steel}}, \tag{5.10}$$

where $\mathrm{NPC}_{\mathrm{steel}}$ is the Net Present Cost normalized by the total steel production over the analysis horizon (\$/t_steel) and $\mathrm{PV}^{\mathrm{CC}}_{\mathrm{steel}}$ is the present value of carbon credits expressed on the same basis. The fraction of the cost per ton offset by carbon credits is then:

$$\eta = \frac{\mathrm{PV}^{\mathrm{CC}}_{\mathrm{steel}}}{\mathrm{NPC}_{\mathrm{steel}}} \cdot 100. \tag{5.11}$$

Figure 5.7 compares $\mathrm{NPC}_{\mathrm{steel}}$ and $\mathrm{NPC}^{\mathrm{net}}_{\mathrm{steel}}$, highlighting the cost reduction associated with carbon credits under the Medium price assumption.

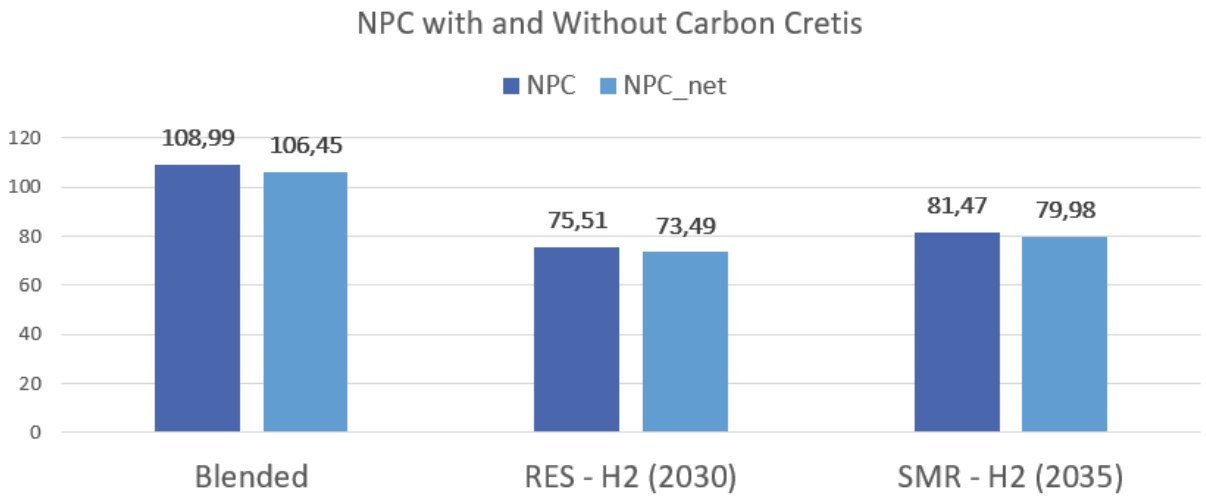

Figure 5.7: Net Present Cost normalized by total steel production, NPCsteel (\$/t_steel), and credit-adjusted cost, NPC$^{\mathrm{net}}$steel = NPCsteel − PV$^{\mathrm{CC}}$steel (Medium carbon price $P = 6.97$ USD/tCO$_2$, $r = 0.05$, 2025–2040).

Table 5.3: Share of incremental NPC offset by discounted carbon-credit revenues under the Medium price assumption.

Scenario	η_s [%]
RES–H_2 (2030)	2.64
SMR–H_2 (2035)	1.81
Blended	2.34

In general, carbon credits offset only about 2% of NPC in the cases analyzed. While this effect is not sufficient to close the cost gap relative to the Baseline, it remains a relevant contribution and can become more significant under higher carbon price assumptions.

5.4. Energy security and supply diversification

This section discusses the implications of supply diversification for the plant, with a focus on security of supply and exposure to fuel-price and geopolitical risks.

To this end, the primary-energy supply mix is computed and compared across the four scenarios for a representative year within the third development step.[1] The mix is expressed in primary-energy terms and covers the full modeled steelmaking route, from ore concentration to the rolling mill.

The primary energy intensity associated with each source i is computed as:

$$e_{\text{prim},i} = \frac{E_{\text{prim},i}}{m_{\text{steel}}} \qquad \left[\frac{\text{MWh}_{\text{prim}}}{\text{t}_{\text{steel}}}\right], \tag{5.12}$$

where $E_{\text{prim},i}$ denotes the primary energy attributed to source i, and P_{steel} is the annual steel production.[2]

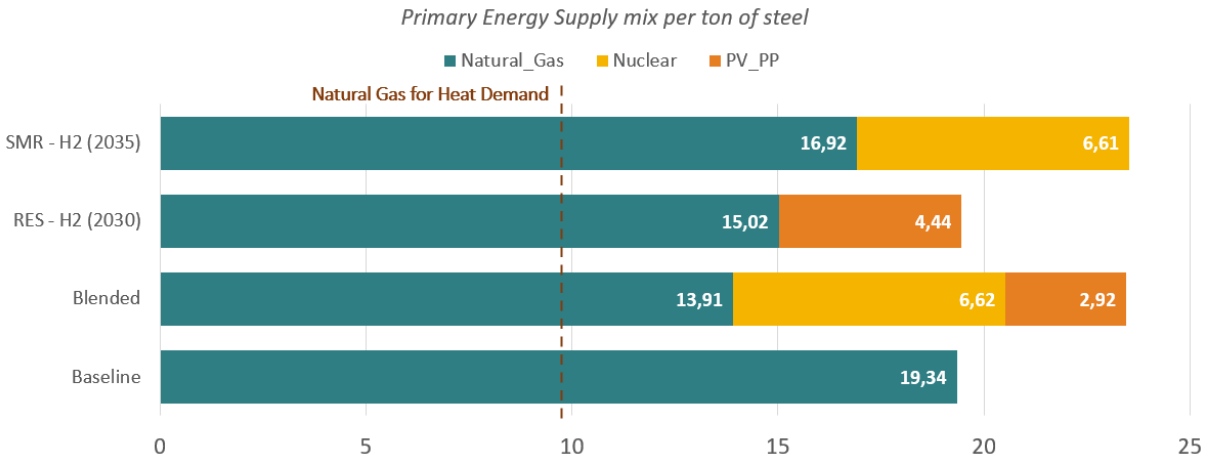

Figure 5.8: Primary-energy supply by source per ton of steel (representative year of Step 3). The dashed line indicates the fixed natural-gas input required to meet process-heat demand, assumed constant across scenarios.

Figure 5.8 shows the primary-energy contribution of each source required to produce one ton of steel, accounting for both heat and electricity needs along the entire production route. Relative to the Baseline case, the decarbonization scenarios reduce the primary-energy contribution of natural gas to different extents, thus implying different degrees of

[1] The choice of the specific year within the step does not affect the results, since production and demand are assumed constant throughout the step.

[2] For nuclear energy, primary energy is reconstructed from useful electricity and heat output by assuming a constant thermal efficiency.

exposure to natural-gas price volatility and supply risks.

> **Key insight.** Hydrogen-based decarbonization pathways affect energy security differently: renewable-based configurations reduce both CO_2 emissions and operational dependence on natural gas, whereas SMR-based configurations mainly reduce carbon intensity while retaining a sizeable natural-gas share in the supply mix.

The main implications of increasing the share of low-carbon sources in the primary-energy mix can be summarized as follows:

- Lower exposure to fossil-fuel price volatility.
- Higher long-term cost predictability, given the low marginal costs of renewable generation.
- Improved alignment with long-term decarbonisation targets.
- Potential constraints related to critical-material supply chains (renewables) and nuclear fuel-cycle services (SMRs).
- Higher system costs at high renewable penetration levels, due to the need for flexibility options and additional capacity.

To complement the intensity-based results, Fig. 5.9 reports the fuel supply in the final development step across scenarios. Natural-gas values include the gas used for both process heat and on-site electricity generation.

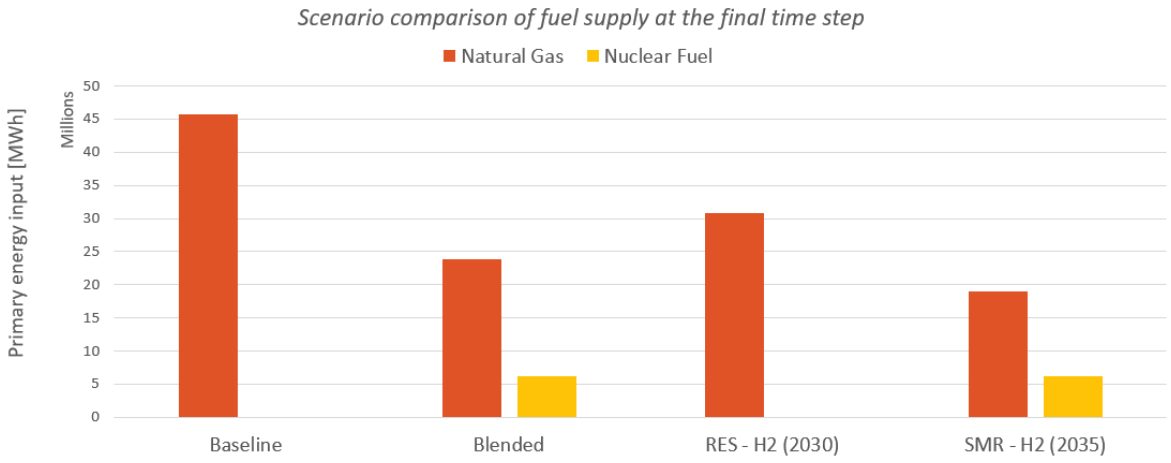

Figure 5.9: Fuel supply at the final time step across scenarios (energy-equivalent).

As shown in the Figure 5.9, natural gas continues to play a non-negligible role in every scenario considered. Even when renewable generation and hydrogen-based options are

introduced, the system still relies on natural gas to ensure operational flexibility and supply adequacy. However, the transition pathways reduce the contribution of natural gas within the hydrogen scenarios.

Bolivia has historically relied on natural gas both as a domestic energy source and as a key export commodity. Recent assessments, however, point to a sustained decline in natural gas production and exports, which has weighed on growth and contributed to external imbalances. In this context, scenarios retaining a high natural-gas share remain more exposed to fuel-price volatility and supply risks than pathways that diversify the primary-energy mix [21].

Similar considerations apply to nuclear fuel supply. In particular, uranium-based generation relies on an international nuclear fuel chain that includes uranium supply, conversion, enrichment, and fuel fabrication. Recent evidence from the literature indicates that Bolivia is developing its nuclear programme through international cooperation; for instance, the RB-01 research reactor project is framed within an agreement between the Russian Federation and the Plurinational State of Bolivia [10].

5.5. Land availability and spatial constraints

Beyond techno-economic performance, the practical deployment of renewable energy and, in this case, utility-scale PV, depends on territorial factors such as solar resource quality and seasonality, land availability, environmental sensitivity, and the need for grid and logistics upgrades. For this reason, a territorial (spatial) assessment is carried out.

The capacity required to meet the plant's energy demand with renewable energy starting from 2030 would require approximately 28 km^2 of land, assuming a PV land-use intensity of about 17 m^2/kW [34].

The available area can be classified as follows:

- **Mining and industrial zones:** The Mutún iron ore deposit (approximately 75 km^2) is primarily dedicated to mining activities and related infrastructure.
- **Existing water bodies:** Laguna Cáceres to the north, together with seasonal wetlands and lagoons, are unsuitable for PV installation [1].
- **Protected areas:** This represents the most critical constraint. Directly south and west of Mutún lies the Otuquis National Park and Integrated Management Natural Area (PN-ANMI Otuquis), which extends over more than 10,000 km^2 of protected Pantanal wetlands [4].

– **Settlements and agriculture:** The surrounding area includes small settlements and agricultural land. Puerto Suárez is located approximately 28 km north of Cerro Mutún, while smaller communities (e.g., San Juan del Mutún) are located much closer to the site.

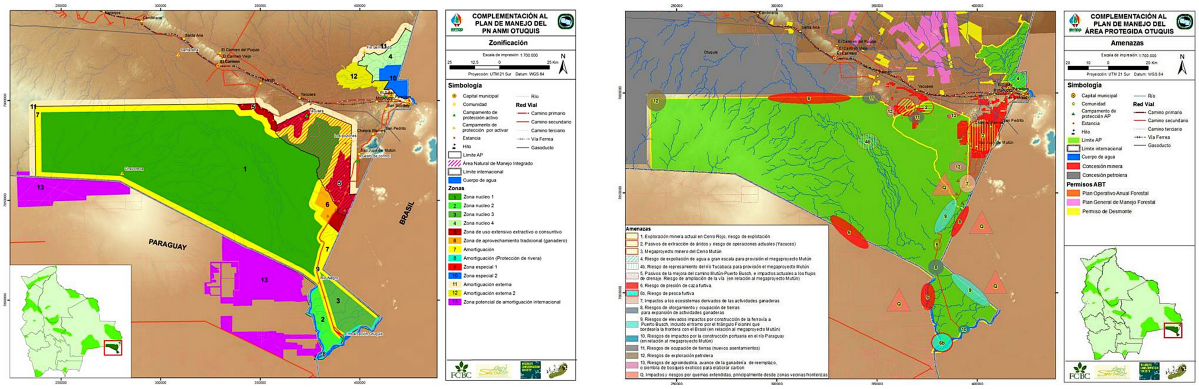

Figure 5.10: Land-use classification of the Mutún territory [42]

As shown in Figure 5.10, the spatial distribution of the aforementioned constraints can be observed. Using the map reference scale, a potentially viable area can be identified in the north-east sector of Mutún. This area has an approximately rectangular shape and an estimated surface of about 22 km^2.

However the Mutún deposit is located within the Gran Pantanal, a fragile ecological region recognised as one of the largest continuous wetland systems in the world [18]. As a result, the feasibility of installing large-scale PV infrastructure in this area cannot be unequivocally confirmed.

While the Renewable scenario presents significant constraints in terms of land availability for PV installation, the Blended scenario requires a substantially smaller surface, approximately 10 km^2, compared to the 28 km^2 required by the RES case.

This makes the Blended scenario more favourable than the RES scenario from a territorial constraint perspective.

5.6. Sensitivity Analysis of SMR Investment Costs

Since the most cost-effective solution identified by the HYPATIA model (which minimizes the Net Present Cost) is based on the deployment of renewable energy technologies, the aim of this section is to investigate the investment cost level at which Small Modular Reactors (SMRs) become economically competitive and are therefore selected by the model instead of renewables.

This analysis is particularly relevant because the SMR investment cost adopted in this study is based on current literature estimates, which are subject to significant uncertainty and may change by 2035. For this reason, a sensitivity analysis on the SMR investment cost is performed to assess the model response to potential cost reductions.

The analysis starts from an SMR investment cost of 3200 $/kW, taken from the literature [13]. Based on this reference value, this section investigates how ΔNPC decreases as the SMR investment cost is reduced.

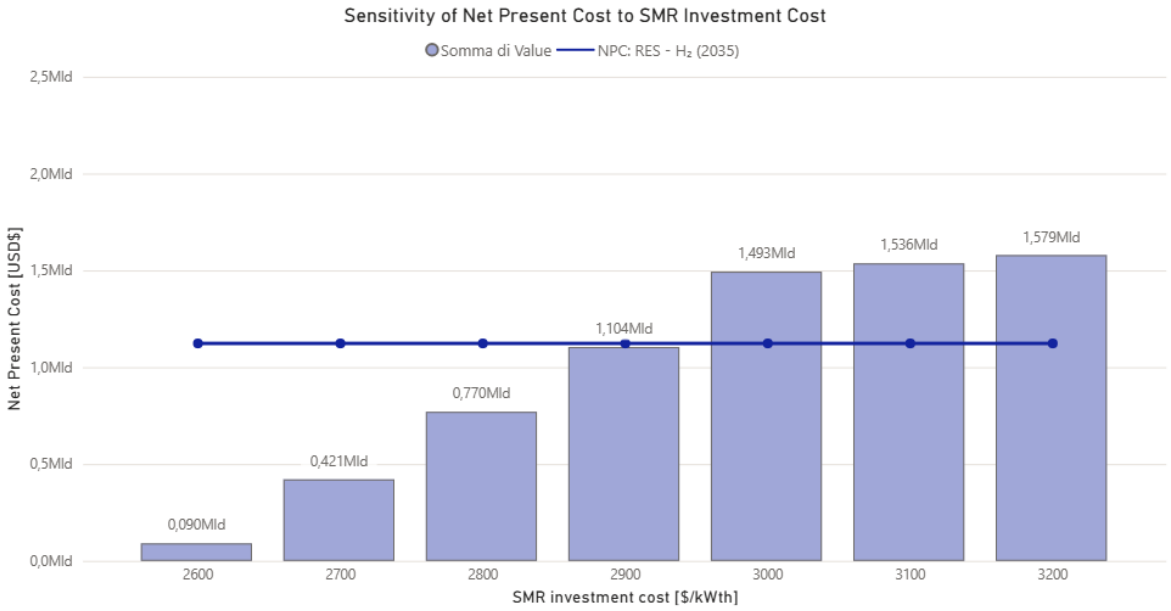

Figure 5.11: Delta Net present cost of the nuclear-based scenario for different SMR investment cost assumptions. The ΔNPC of the RES–H_2 (2030) scenario is also reported for comparison.

By further decreasing this cost, it is observed that the threshold value enabling the installation of SMRs instead of renewable energy is relatively close to current cost estimates, consistently with the limited difference in net present cost between the RES–H_2 (2035) and SMR–H_2 (2035) scenarios.

An optimal SMR investment cost of approximately 2900 $/kW is identified. This value appears reasonable, considering the uncertainty associated with current SMR cost projections and their potential reduction through technological learning and deployment.

This simulation leads to the following configuration:

– The installed capacity remains the same, since the demand is unchanged and the only variable considered in this analysis is the SMR investment cost.

- The share of green electricity and the total CO_2 emissions correspond to those of the SMR–H_2 (2035) scenario.
- The analysis focuses on economic performance, as the investment cost is the only parameter varied in this scenario.

5.7. Discussion

This section provides a comparative overview of the analyzed scenarios for the *Empresa Siderurgica Del Mutùn* and presents a discussion that links the key indicators presented in previous section to their underlying drivers and practical constraints, highlighting the main trade-offs across configurations and the implications for technology deployment, operational feasibility, and integration with the plant's energy and material flows. The discussion also clarifies how differences in resource availability, conversion efficiencies, and system boundaries translate into the observed indicator trends across the considered time horizons.

Scenario overview and timing (H_2 introduction)

- **Baseline:** NG-based DRI in all steps; only capacity expansion (no H_2).
- **RES–H_2 (2030):** H_2-based DRI from **2030** (Step 2) via *PEM + RES + Battery*; same configuration in Step 3.
- **SMR–H_2 (2035):** NG-based DRI until **2035**; H_2-based DRI only in Step 3 via *SMR + SOEC*.
- **Blended:** H_2-based DRI from **2030** (*PEM + RES + Battery*); in Step 3 adds *SMR + SOEC + Battery*.

Supply structure

- **Operational role of NG engines:** in RES/Blended they shift away from continuous operation toward balancing/reserve, while in SMR–H_2 they remain highly utilised.
- **Electricity/H_2 split:** the Sankey comparison highlights that later SMR deployment leads to a higher NG share during the transition period.

Cost vs emissions

- **Emissions (CO_2 intensity / total CO_2):** Baseline is the highest emitter; hydrogen-based scenarios deliver comparable reductions, with the Blended case

achieving the lowest emissions among H_2 pathways.

- **Costs (ΔNPC: Additional investment compared to the Baseline Case):** all H_2 configurations increase NPC versus Baseline due to new H_2 production and infrastructure; RES–H_2 and SMR–H_2 show a relatively small NPC difference, whereas Blended is the highest-cost portfolio.
- **Cost-effectiveness (Cost of avoided CO_2):** the ranking should be read jointly: the "best" emissions outcome does not necessarily correspond to the lowest avoided-cost, especially when multiple technologies are deployed simultaneously.

Feasibility and supply-risk reflections

- **Land use (km^2 required):** RES–H_2 requires large PV area (high land requirement), while Blended needs substantially less land, improving territorial feasibility.
- **Natural gas outlook (risk dimension):** scenarios retaining a high NG share remain exposed to price volatility and supply risks in a context of declining Bolivian gas production/export prospects.
- **Nuclear fuel chain (risk dimension):** SMR deployment implies reliance on an international uranium fuel cycle (supply, conversion, enrichment, fabrication) and related geopolitical/logistic dependencies.

Summary

- **If the priority is minimizing cost alone:** Baseline remains cost-optimal but fails on emissions and NG exposure.
- **If the priority is minimum NG dependence / higher energy security:** RES–H_2 and Blended are favoured (earlier diversification).
- **If emissions are a priority**: under this criterion, all configurations involving hydrogen introduction achieve a substantial reduction in plant emissions.
- **If land is the binding constraint:** Blended is more feasible than a fully RES-based pathway.
- **Conditions that can shift the ranking**: SMR competitiveness is highly sensitive to investment assumptions. In addition, policy mechanisms as carbon credits can partially offset the additional costs associated with hydrogen-based pathways, especially if the Bolivian government were to adopt a high carbon price.

6 | Conclusions

In the context of the climate challenge, decarbonizing hard-to-abate sectors such as steelmaking is crucial. Among the possible mitigation pathways, hydrogen represents a key option: it can reduce emissions by replacing carbon-based reducing agents in iron ore reduction and, at the same time, support the diversification of the energy mix required to supply both hydrogen production and the electricity demand of the steel plant.

In this work, hydrogen-based pathways are modeled through the substitution of natural gas as reducing gas in the Direct Reduced Iron (DRI) process.

Two main supply options are investigated. The first relies on renewable electricity coupled with low-temperature water electrolysis, modeled as PEM electrolysis. The second considers small modular reactors (SMRs), i.e., nuclear reactors with a standard electrical output of about 300 MW_{el} and a power cycle configuration comparable to conventional nuclear power plants, coupled with high-temperature electrolysis (SOEC).

In the nuclear-based configuration, the SMR is assumed to provide both electricity and heat. The thermal output is used to support SOEC electrolysis in order to meet the additional hydrogen demand, while the remaining electric power contributes to covering the plant electricity consumption, similar to the case based on renewables. An advanced SMR concept is considered in the model (specifically, an HTGR). However, the reactor thermal output is not sufficient to meet the high-temperature heat requirements of the steelmaking facility; therefore, nuclear heat is assumed to be utilised exclusively for SOEC electrolysis.

The main objective of this study is to assess the feasibility of these pathways for the *Empresa Siderúrgica del Mutún*, a steelmaking facility in Bolivia, which exploits one of the largest iron ore deposits in the world. The analysis is carried out using the Energy System Optimisation Modelling framework *Hypatia*.

First, the current state of the facility is described through its Reference Energy System, current energy demand, and expected demand growth. The evolution is represented through three development steps covering the 2025–2040 horizon. To enable the as-

sessment of hydrogen integration, the hydrogen demand required to meet the growing production levels is estimated accordingly.

The following scenarios are considered:

- **Baseline:** reference configuration without hydrogen introduction;
- **RES–H_2 (2030):** renewable electricity supply with hydrogen introduction from 2030;
- **SMR–H_2 (2035):** SMR-based supply with hydrogen introduction from 2035;
- **Blended:** combined RES and SMR portfolio (RES from 2030 and SMR from 2035), with hydrogen introduced from 2030.

Scenario results are then compared and discussed. As expected, the introduction of hydrogen leads to a significant reduction in CO_2 emissions, but also to an increase in overall system costs due to the additional investments required for hydrogen production and integration. The potential contribution of carbon credits, which could partially support the decarbonization effort of the *Empresa Siderúrgica del Mutún*, is also evaluated. Finally, the discussion includes feasibility aspects beyond techno-economics, such as territorial constraints (e.g., land availability for renewables) and fuel supply-chain considerations relevant to the *Plurinational State of Bolivia*.

Overall, the aim is to highlight strengths and weaknesses of the proposed configurations and to identify the most suitable solution for the case study. The main conclusion can be summarized:

(i) **Hydrogen enables a structural reduction in emissions.** Introducing hydrogen in the DRI stage leads to a substantial decrease in CO_2 emissions, exceeding a 50% reduction relative to the Baseline configuration. All three hydrogen pathways deliver broadly comparable decarbonisation outcomes; among them, the Blended portfolio achieves the lowest emissions, reaching a 70% reduction versus the baseline in the final development step of the analysis.

(ii) **Transition timing determines natural-gas exposure over 2025–2040.** Scenarios with earlier hydrogen deployment (RES–H_2 and Blended from 2030) reduce system reliance on natural gas over the transition period by roughly half. Conversely, the SMR–H_2 case retains a higher natural-gas share prior to SMR commissioning in 2035, resulting in greater exposure during the intermediate years, with only a 27% reduction relative to the baseline.

(iii) **Decarbonisation comes with a clear cost premium, and rankings depend on cost-effectiveness.** All hydrogen-based scenarios increase total costs due to additional investments in hydrogen production and integration; depending on the case, the overall plant cost is nearly doubled along the hydrogen pathways. Therefore, scenario selection should be based on a combined assessment of emissions reductions and cost-effectiveness, rather than on a single indicator.

(iv) **Technology portfolios.** Renewable-heavy configurations require storage and flexibility to manage intermittency, while SMR-based pathways require the integration of nuclear generation with high-temperature electrolysis.

(v) **Practical feasibility constraints can dominate the final preference.** Large-scale RES deployment entails substantial land requirements, which may become a binding constraint. Accordingly, the two configurations that rely on RES may need to be adjusted to local land availability; in particular, the Blended case, which requires a smaller installed PV capacity than the RES–H_2 case, is likely to be more readily implementable under land constraints.

At the same time, configurations with high dependence on natural gas remain exposed to fuel supply and price risks, while SMR deployment introduces additional considerations related to the nuclear fuel supply chain. Notably, all four scenarios retain a non-negligible reliance on natural gas; however, the hydrogen-based configurations achieve a more diversified energy mix per ton of steel produced, which is beneficial from an energy-security perspective.

As a result, the most suitable pathway for the *Empresa Siderurgica Del Mutùn* depends on the prioritization of objectives (emissions vs cost) and on the binding feasibility constraints (land availability, fuel-chain risks, and implementation complexity).

Bibliography

[1] Bolivia. *IEA*. URL https://www.iea.org/countries/bolivia/renewables#what-are-the-main-sources-of-renewable-heat-in-bolivia.

[2] La industria del hierro. *ERBOL*. URL https://erbol.com.bo/medio-ambiente/en-bolivia-la-industria-del-hierro-se-abre-paso-en-los-humedales-del-pantanal.

[3] Hydrogen's potential for onshoring australian green iron production. *Institute for Energy Economics and Financial Analysis*. URL https://ieefa.org/articles/hydrogens-potential-onshoring-australian-green-iron-production.

[4] Bolivia. *Protected Planet*. URL https://www.protectedplanet.net/country/BOL.

[5] *Case study on the impact of cogeneration and thermal storage on the flexibility of the power system*. Publications Office, 2018. URL https://publications.jrc.ec.europa.eu/repository/handle/JRC110285.

[6] Paying for quality, 2023. URL https://3298623.fs1.hubspotusercontent-na1.net/hubfs/3298623/SOVCM%202023/2023-EcoMarketplace_SOVCM-Nov28_FINALrev-Mar2024.pdf.

[7] Steel: an enabler and a threat to the energy transition. *Vitol*, 2024. URL https://www.vitol.com/steel-an-enabler-and-a-threat-to-the-energy-transition-vitols-view/.

[8] Bolivia to issue sovereign credits in 2026, completing dramatic shift toward carbon markets. Carbon Pulse, Aug. 2025. URL https://carbon-pulse.com/423114/. Published 2025-08-01; Accessed 2026-02-17.

[9] Overview of carbon pricing policies in latin america and the caribbean 2025: analysis of their effects and related policies. Technical report, Economic Commission for Latin America and the Caribbean (ECLAC/CEPAL), 2025. URL https://capacity4dev.europa.eu/media/281828/download/ff5384ee-3b8b-4abb-b8cd-242b27b09f67_en. Accessed 2026-02-17.

[10] I. A. E. Agency. Iaea completes integrated safety as-

sessment mission for bolivia's first nuclear research reactor, 2025. URL https://www.iaea.org/newscenter/pressreleases/iaea-completes-integrated-safety-assessment-mission-for-bolivias-first-nuclear-rese

[11] H. I. Ali Hasanbeigi, Cecilia Springer. Green h2-dri steelmaking: 15 challenges and solutions. Technical report, 2014. URL https://www.globalefficiencyintel.com/green-h2-dri-steelmaking-15-challenges-and-solutions.

[12] W. S. Association. Water management in the steel industry. *World Steel Association*, pages 2–41, 2011. URL https://worldsteel.org/media/publications/water/.

[13] A. Asuega, B. J. Limb, and J. C. Quinn. Techno-economic analysis of advanced small modular nuclear reactors. *Applied Energy*, 334:120669, 2023. ISSN 0306-2619. doi: https://doi.org/10.1016/j.apenergy.2023.120669.

[14] G. S. Atlas. Bolivia, 2024. URL https://globalsolaratlas.info/download/bolivia.

[15] G. S. Atlas. Bolivia, 2024. URL https://globalwindatlas.info/en/area/Bolivia.

[16] O. Benedikt, P. Sucha, and Z. Hanzálek. On idle energy consumption minimization in production: Industrial example and mathematical model. 2020. URL https://arxiv.org/abs/2005.06270.

[17] S. L. de Moraes, J. R. B. de Lima, and T. R. Ribeiro. Iron ore pelletizing process: An overview. 2018. URL https://www.intechopen.com/chapters/58868.

[18] DialogueEarth. In bolivia, a new industry dawns in the threatened pantanal wetlands, 2024. URL https://dialogue.earth/en/business/in-bolivia-a-new-industry-dawns-in-the-threatened-pantanal-wetlands/#:~:text=The%20Bolivian%20Pantanal%2C%20located%20on,continuous%20wetland%20in%20the%20world.

[19] ENERGIRON. A technology for flexible solutions, 2022. URL https://www.energiron.com/solutions?utm_source.

[20] S. Fujiwara, S. Kasai, H. Yamauchi, K. Yamada, S. Makino, K. Matsunaga, M. Yoshino, T. Kameda, T. Ogawa, S. Momma, and E. Hoashi. Hydrogen production by high temperature electrolysis with nuclear reactor. *Progress in Nuclear Energy*, 2008. URL https://www.sciencedirect.com/science/article/abs/pii/S0149197007001709?via%3Dihub.

[21] I. M. Fund. Bolivia: Imf executive board concludes 2024 article iv consultation with bolivia, 2025. URL https://www.imf.org/en/news/articles/2025/01/28/pr25018-bolivia-imf-executive-board-concludes-2024-article-iv-consultation-wit

[22] B. Gajdzik, R. Wolniak, and W. W. Grebski. Electricity and heat demand in steel industry technological processes in industry 4.0 conditions. *Energies*, 16(2), 2023. URL https://www.mdpi.com/1996-1073/16/2/787.

[23] Global Energy Monitor. Esm mutún steel plant, 2025. URL https://www.gem.wiki/ESM_Mut%C3%BAn_steel_plant#Location.

[24] IEA. Iron and steel technology roadmap. 2020. URL https://www.iea.org/reports/iron-and-steel-technology-roadmap.

[25] M. Jaszczur, M. Dudek, and Z. Kolenda. Thermodynamic analysis of advanced gas turbine combined cycle integration with a high-temperature nuclear reactor and cogeneration unit. *Energies*, 13(2), 2020. doi: 10.3390/en13020400. URL https://www.mdpi.com/1996-1073/13/2/400.

[26] E. Jean Milien, G. M. Nunes, G. Pierre, S. K. Hamilton, and C. N. Da Cunha. Hydrological dynamics of the pantanal, a large tropical floodplain in brazil, revealed by analysis of sentinel-2 satellite imagery. *Water*, 15(12), 2023. URL https://www.mdpi.com/2073-4441/15/12/2180.

[27] V. Kindra, I. Maksimov, O. Zlyvko, A. Rogalev, and N. Rogalev. Thermodynamic analysis and comparison of power cycles for small modular reactors. *Energies*, 17(7), 2024. ISSN 1996-1073. doi: 10.3390/en17071650.

[28] L. Kotzur, P. Markewitz, M. Robinius, and D. Stolten. Impact of different time series aggregation methods on optimal energy system design. *Renewable Energy*, 117:474–487, 2018. ISSN 0960-1481. doi: https://doi.org/10.1016/j.renene.2017.10.017. URL https://www.sciencedirect.com/science/article/pii/S0960148117309783.

[29] C. Lamy. From hydrogen production by water electrolysis to its utilization in a pem fuel cell or in a so fuel cell: Some considerations on the energy efficiencies. *International Journal of Hydrogen Energy*, 2016. URL https://www.sciencedirect.com/science/article/abs/pii/S0360319916304232?via%3Dihub.

[30] M. A. K. M. P. M. T. E. T. C. D. Layzell. Hydrogen and the decarbonization of steel production in canada: Reaching economies of scale. *Energy Transitions Commission*, 2023. URL https://www.energy-transitions.org/publications/hydrogen-decarbonisation-steel-production-canada/.

[31] G. Locatelli, C. Bingham, and M. Mancini. Small modular reactors: A comprehensive overview of their economics and strategic aspects. *Progress in Nuclear Energy*, 73: 75–85, 2014. ISSN 0149-1970. doi: https://doi.org/10.1016/j.pnucene.2014.01.010.

[32] J. Madias. *Electric Furnace Steelmaking*, pages 243–265. 01 2024. ISBN 9780323853736. doi: 10.1016/B978-0-323-85373-6.00021-1.

[33] H. Maximilian and K. Leander. Tsam: time series aggregation module. URL `https://tsam.readthedocs.io/en/latest/`.

[34] S. Ong, C. Campbell, P. Denholm, R. Margolis, and G. Heath. Land-use requirements for solar power plants in the united states. Technical Report NREL/TP-6A20-56290, National Renewable Energy Laboratory (NREL), June 2013. URL `https://docs.nlr.gov/docs/fy13osti/56290.pdf`.

[35] G. Parker. Encyclopedia of materials: Science and technology. *Elsevier*, 2001. URL `https://eprints.soton.ac.uk/259958/`.

[36] E. P. R. Service. Carbon-free steel production, cost reduction options and usage of existing gas, 2021. URL `https://www.europarl.europa.eu/RegData/etudes/STUD/2021/690008/EPRS_STU(2021)690008_EN.pdf`.

[37] W. Sun, Q. Wang, Y. Zhou, and J. Wu. Material and energy flows of the iron and steel industry: Status quo, challenges and perspectives. *Applied Energy*, 268:114946, 2020. ISSN 0306-2619. doi: https://doi.org/10.1016/j.apenergy.2020.114946.

[38] H. team. Hypatia | energy modelling framework. URL `https://tsam.readthedocs.io/en/latest/`.

[39] TERI. Energy efficient technologies and best practices in steel rolling industries (indonesia). Technical report, The Energy and Resources Institute (TERI) / United Nations Environment Programme (UNEP), 2014. URL `https://www.sameeeksha.org/books/Manual-on-Energy-Efficiency.pdf`.

[40] Wikipedia. Puerto suárez, 2025. URL `https://en.wikipedia.org/wiki/Puerto_Su%C3%A1rez`.

[41] X. Wu. Technological pathways for cost-effective steel decarbonization. *Nature*, 2025. URL `https://www.nature.com/articles/s41586-025-09658-9#citeas`.

[42] P. N. y Área Natural de Manejo Integrado. Plan de monitoreo, 2022. URL `https://fcbc.org.bo/wp-content/uploads/2016/10/Plan-monitoreo-Otuquis.pdf`.

[43] T. Zacconi. Evaluating the nuclear role in the italian power sector: scenario analysis

by means of energy system modelling. Technical report, Politecnico di Milano, 2024. URL https://hdl.handle.net/10589/230392.

A | Appendix A

	Residual Capacity [MW]
NG_Power	103
NG_Heat	180

Table A.1: Already installed capacity in the *Empresa Siderúrgica del Mutún* at the beginning of the modeling period 2025.

	INV [€/kW]	F_O&M [€/kW/y]	V_O&M [€/kWh]
Solar_PV	750	10,48	0
Wind_PP	1300	37,3	0
SMR	3100	65	0,00338
SMR_Power	3100	65	0,00338
NG_Power	850	27,5	0,0064
PEM	see Table A.3	22,5	0
SOEC	see Table A.3	25,5	0
Battery Storage	345	30	0

Table A.2: Economic input parameters by technology

Year	PEM [€/kW]	SOEC [€/kW]
2030	1500,56	1700,56
2031	1470,43	1670,43
2032	1435,76	1635,76
2033	1399,71	1599,71
2034	1367,62	1567,62
2035	1333,78	1533,78
2036	1292,88	1492,88
2037	1256,88	1456,88
2038	1210,88	1410,88
2039	1178,22	1378,22
2040	1145,98	1345,98
2041	1110,88	1310,88
2042	1099,89	1299,89
2043	1064,99	1264,99
2044	1024,55	1224,55
2045	986,89	1186,89

Table A.3: Investment costs assumed for PEM and SOEC electrolysis (2030–2050).

B | Appendix B

The SMR was implemented in Hypatia following the scheme reported in B.1

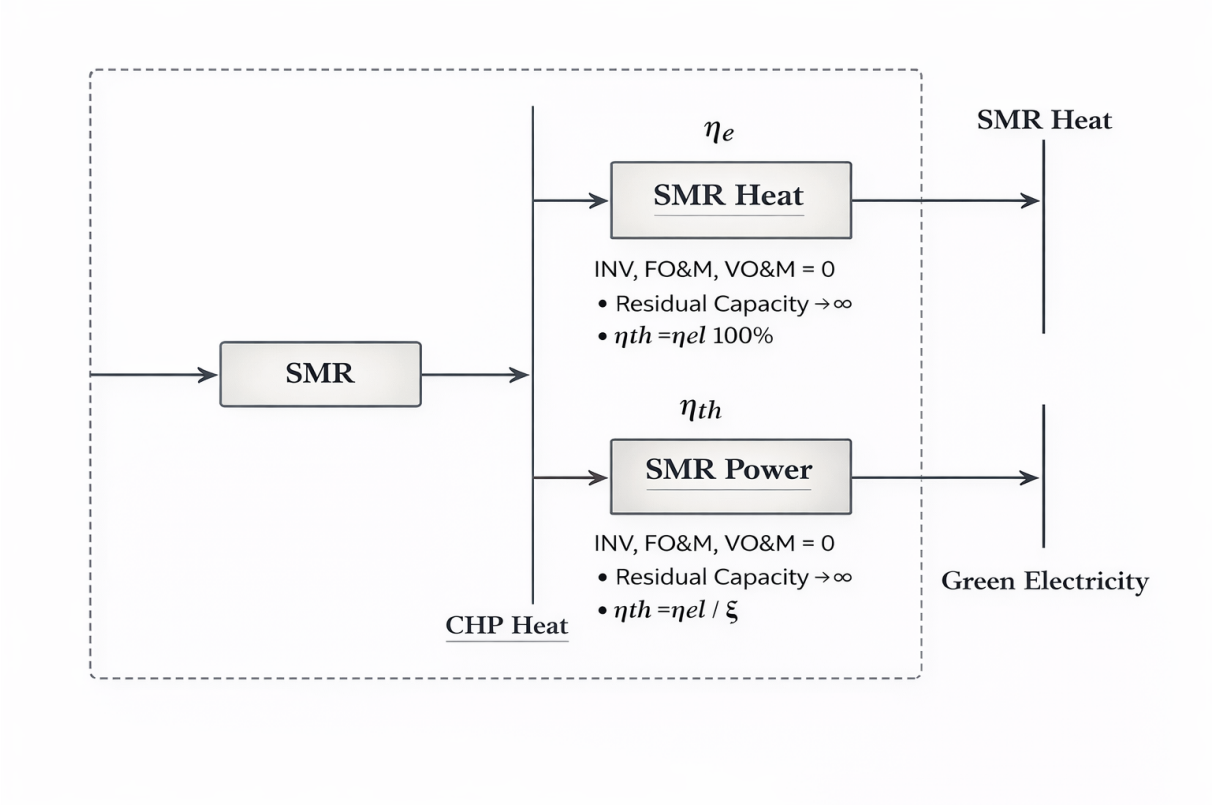

Figure B.1: SMR cogenerative modeling framework implemented in Hypatia

List of Figures

1.1 Schematic comparison of the BF–BOF, DR–EAF, and H–DR–EAF steelmaking routes [11]. 2

2.1 Simplified steelmaking route with representative equipment sketches for each process step. 8
2.2 Natural gas-based DRI and Pink/Green Hydrogen-based DRI configurations [3]. 10

3.1 Schematic representation of the Hypatia modelling framework, highlighting operational and planning modes. 18
3.2 Block representation of the adopted time-series aggregation (clusters and weights). 21
3.3 Workflow used to integrate TSAM representative periods with additional manually selected clusters and to compute consistent time fractions. 22
3.4 Hourly solar availability over the representative 72-hour period for each cluster. 23
3.5 Feasible operating region of the SMR CHP unit. 25

4.1 Geographical location of the Empresa Siderúrgica del Mutún in Bolivia. Source: Google Maps. 27
4.2 Long-term average Global Horizontal Irradiation (GHI) in Bolivia [14]. . . 28
4.3 Long-term mean wind speed at 100 m in Bolivia. Source: Global Wind Atlas v3.3 (DTU/World Bank/ESMAP). 29
4.4 Current Reference Energy System of the Plant 30
4.5 Hourly electrical power demand of the steel plant. The upper panel shows the full operating range, while the lower panel provides a zoomed-in view highlighting the small fluctuations. 33
4.6 Scenario pathways across development steps (technology configuration adopted in each time window). 35
4.7 Updated reference energy systems for hydrogen production 36

4.8 Hydrogen demand and steel production by development step (30% H_2 in DRI). 38

5.1 Installed capacity in the third development step 39
5.2 Normalized Sankey diagrams (shares, %) showing the breakdown of primary energy inputs to electricity and hydrogen production over 2025–2040 for the three hydrogen scenarios. In each diagram, all flows are expressed as fractions of the total energy input to the electricity+H_2 supply chain, hence the incoming flows sum to 100%. 41
5.3 CO_2 emissions per ton of steel produced. 43
5.4 Percentage reduction in total CO_2 emissions across scenarios relative to the Baseline case. 44
5.5 Net Present Cost (NPC) normalized by the total steel production over the analysis horizon (\$/t_steel) for each scenario. Higher values indicate scenarios with higher cost per ton of steel. 45
5.6 Cost of avoided CO_2. 46
5.7 Net Present Cost normalized by total steel production, NPCsteel (\$/t_steel), and credit-adjusted cost, $NPC^{net}steel = NPCsteel - PV^{CC}steel$ (Medium carbon price $P = 6.97$ USD/tCO_2, $r = 0.05$, 2025–2040). 48
5.8 Primary-energy supply by source per ton of steel (representative year of Step 3). The dashed line indicates the fixed natural-gas input required to meet process-heat demand, assumed constant across scenarios. 49
5.9 Fuel supply at the final time step across scenarios (energy-equivalent). . . . 50
5.10 Land-use classification of the Mutún territory [42] 52
5.11 Delta Net present cost of the nuclear-based scenario for different SMR investment cost assumptions. The ΔNPC of the RES–H_2 (2030) scenario is also reported for comparison. 53

B.1 SMR cogenerative modeling framework implemented in Hypatia 69

List of Tables

2.1 Typical operating temperature of existing SMR technologies [27] 12

3.1 Main decision variables of the Hypatia model. 17
3.2 Main input parameters of the Hypatia model. 17
3.3 Derived outputs of the Hypatia model. 18
3.4 Key parameters adopted for the SMR CHP model (Hypatia Type 3). . . . 25

4.1 Steel plant electrical demand evolution by process and development step . 31
4.2 Thermal demand of the steelmaking facility 32
4.3 Steel plant thermal demand evolution by process and development step . . 32
4.4 Water consumption per process phase 34

5.1 NG_Power capacity factors by development step for the analysed scenarios. 40
5.2 Carbon credit price assumptions used for scenario analysis (voluntary carbon market). [6] 47
5.3 Share of incremental NPC offset by discounted carbon-credit revenues under the Medium price assumption. 48

A.1 Already installed capacity in the *Empresa Siderúrgica del Mutún* at the beginning of the modeling period 2025. 67
A.2 Economic input parameters by technology 67
A.3 Investment costs assumed for PEM and SOEC electrolysis (2030–2050). . . 68

Acknowledgements

I would like to thank Prof. Stevanato for supervising this work and for the valuable feedback provided throughout the thesis.

I am especially grateful to my co-advisor Tommaso, whose guidance was truly fundamental. He supported me step by step, sharing crucial insights and lessons, and contributing decisively to the quality of this work.